Plant Growth Regulation (2026) 106:46
https://doi.org/10.1007/s10725-026-01447-2

ORIGINAL PAPER

Integrated eco-friendly management of *Meloidogyne incognita* in greenhouse-grown tomato via grafting onto resistant rootstocks and bacterial bioagent seed coating

Ahmed M.A. Mahmoud[1] · Neama H. Osman[2] · Ahmed A.S.A. El-Eslamboly[3] · Mohamed Adam[4] · Mahmoud A.A. Maraey[1]

Received: 27 November 2025 / Accepted: 14 March 2026

Abstract

This study explored an eco-friendly, integrated strategy for managing root-knot nematode (RKN; *Meloidogyne incognita*) in greenhouse-grown tomato cv. Apache F_1. The strategy combined grafting (GR) onto resistant rootstocks ('Estamino': R_1 and 'Fortamino': R_2) with seed coating (SCB) using bacterial bioagent *Sporosarcina psychrophila* Sd4-11 (B_1) and *Streptomyces scabiei* Wb1n-4 (B_2). Grafted and ungrafted transplants, with or without seed coating, were cultivated in a naturally infested greenhouse during the 2022 and 2023 fall seasons using a randomized complete block factorial design. Comprehensive assessments were performed for host RKN-response, vegetative and reproductive performance, yield attributes, fruit quality, and metabolic activity, thereby addressing existing knowledge gaps regarding the combined efficacy of grafting and biocontrol strategies. The integrated GR-SCB approach significantly enhanced vegetative and reproductive growth, productivity, and metabolic activity, with markedly reducing RKN-infection. Analysis of variance revealed significant main and interaction (GR×SCB) effects across most measured traits, with seasonal and trait-specific variation. SCB most effectively suppressed RKN-satisfying response (number of galls and egg masses), whereas GR exerted the strongest influence on vegetative traits. The GR×SCB interaction contributed the highest proportion of variance in yield attributes (SS%: approximately 40–45%), confirming the synergistic potential. Principal component analysis (PCA) reduced 37 evaluated traits to three principal components explaining 97.06% of the total variance. PCA biplot results identified G-R_1/C-B_1 and G-R_1/C-B_2 as the most vigorous and RKN-tolerant combinations. Overall, integrating grafting with bioagent seed coating provides an effective, sustainable, and eco-friendly alternative to chemical nematicides for enhancing tomato productivity under protected cultivation.

Keywords Polyphenols · Principal Component Analysis · Root-Knot Nematode · *Solanum lycopersicum* · Vegetative Growth · Yield

Abbreviations

AFW	average fruit weight
ANOVA	analysis of variance
BCA	biological control agent
C-B_1	seed-coating with *Sporosarcina psychrophil*e Sd4-11 (B_1)
C-B_2	seed-coating with *Streptomyces scabie*i Wb1n-4 (B_2)
Chlor-a	chlorophyll a
Chlor-b	chlorophyll b
DAT	days after transplanting
DFFE	days to the first flower anthesis
DFRFE	days to the ripening of the first ripe fruit

Communicated by Abhijeet Shankar Kashyap

✉ Ahmed M.A. Mahmoud
ahmed.ali@agr.cu.edu.eg

[1] Vegetable Crops Department, Faculty of Agriculture, Cairo University, Giza 12613, Egypt

[2] Genetics Department, Faculty of Agriculture, Cairo University, Giza 12613, Egypt

[3] Horticulture Research Institute, Agriculture Research Center, Giza, Egypt

[4] Department of Zoology and Nematology, Faculty of Agriculture, Cairo University, Giza 12613, Egypt

Published online: 22 April 2026

EMI	egg-mass index
EU	experimental unit
EY	early yield
FDM	fruit dry matter content
FF	fruit firmness
FSP	fruit set percentage
GI	gall index
GR	grafting
G-R_1	grafting onto rootstock 'Estamino'
G-R_2	grafting onto rootstock 'Fortamino'
INM	integrated nematode management
J_2	second-stage juveniles of nematode
LA	leaf area
LB	Luria-Bertani medium
LER	leaf expansion rate
LFR	leaf formation rate
MY	marketable yield
NEM	number of egg-masses
NFC	the number of fruits/cluster
NFI	the number of flowers/inflorescence
NG	number of galls
NPL	number of plant leaves
PC	principal component
PCA	principal component analysis
P_i	initial population density
RC	root carbohydrates
RCBD	randomized complete block design
RDM	root dry matter
RKN	root-knot nematode
RPPh	root polyphenol content
RPr	root protein content
SCB	seed-coating with bioagent
SD	stem diameter
SDM	shoot dry matter
SER	stem elongation rate
SL	stem length
STR	stem thickness rate
T-Carot	total carotenoids
TSS	total soluble solids
TY	total yield
VC	vitamin C

Introduction

Tomato (*Solanum lycopersicum* L.) is a globally important vegetable crop valued for its nutritional content, antioxidants, flavor, and versatility. In 2023, the worldwide cultivation area reached 4.92 million hectares, producing 192.32 million tons with an average yield of 35.5 tons per hectare (<http://faostat.fao.org/%3E). Egypt ranked the fifth-largest producer worldwide with 6.21 million tons produced in 2023 from 155,874 hectares, averaging 39.85 tons per hectare (<http://faostat.fao.org/%3E). Plant-parasitic nematodes significantly affect tomato crop, causing yield losses of 30–40%, and can reach up to 85% in susceptible cultivars, particularly in tropical and sub-tropical regions (Lopes-Caitar et al. 2019). In Egypt, root-knot nematodes (RKN; *Meloidogyne* spp.), especially *M. incognita*, pose major challenges to intensive tomato production (Abd-Algawad 2014).

Nematode control is complex and costly, with limited effective options. Integrated nematode management (INM) for RKN in sustainable agriculture relies on four key strategies: host plant resistance, cultural practices, biological control, and chemical control. While chemical nematicides can reduce RKN damage, their high cost and potential risks to human health and the environment limit their adoption (Castellano-Hinojosa et al. 2022). Alternatively, grafting onto resistant rootstocks and biological control agents has proven effective in managing RKN and other soil-borne diseases without reliance on chemical pesticides (Remzeena and Anitha 2023; Sharma et al. 2025).

Several commercial tomato rootstocks, primarily interspecific F_1 hybrids with *S. habrochaites*, carry the RKN-resistant gene *Mi*−1, derived from *S. peruvianum* (Aydinli and Mennan 2019; Mahmoud et al. 2025b). The *Mi-1* gene confers resistance to *M. incognita*, *M. javanica*, and *M. arenaria*, as well as some arthropods (El-Sappah et al. 2019). Its effectiveness, however, declines when heterozygous, in the presence of virulent nematode isolates, or at soil temperatures above 32 °C (Devran et al. 2010). Therefore, rootstocks homozygous for *Mi-1*, such as 'Brigeor', 'King Kong', and 'He-Man', exhibit high RKN resistance, whereas heterozygous rootstocks like 'Beaufor', 'Maxifort', 'Estamino', and 'Fortamino' show moderate resistance (Aydinli and Mennan 2019; Mahmoud et al. 2025b). Grafting tomato onto these RKN-resistant rootstocks reduces root galling and nematode reproduction, resulting in significant yield gains compared to ungrafted plants (Aydinli and Mennan 2019; Bajek and Rudolph 2023; Kokalis-Burelle and Rosskopf 2011; Mahmoud et al. 2025b; Owusu et al. 2016).

Indigenous soil microbial communities show potential for controlling *Meloidogyne* spp. Several bacterial genera, species, and isolates that naturally suppress these nematodes have been identified. Rhizosphere bacteria/isolates such as *Bacillus* (Amorim et al. 2024; Jiménez-Aguirre et al. 2023; Mahmoud et al. 2025a), *Paenibacillus* (Viljoen et al. 2019), *Pseudomonas* (Amorim et al. 2024), and *Streptomyces* (Mahmoud et al. 2025a; Sharma et al. 2019) have been successfully used as biological control agents (BCAs) in vegetable crops, including tomato. BCAs act directly—through competition, predation, and parasitism at various nematode life stages—or indirectly by producing nematicidal

metabolites and inducing plant resistance (Sharma et al. 2025). However, their use can be controversial, as non-target soil microorganisms and host plants may be affected, and most beneficial plant–microbe interactions are highly specific, with few broad-spectrum antagonists identified (Sharma et al. 2025).

Although the individual effects of bioprotection and grafting in mitigating RKN damage are well-documented, their synergistic potential remains under-explored. Cukrov et al. (2021) reported that integrating grafting and biostimulant application was a promising strategy for *M. incognita* management in tomato, however, they noted that efficacy s highly dependent on rootstock selection, with 'Arnold' providing superior suppression compared to 'Maxifort'. Similarly, Pontes et al. (2024) found that while microbiological nematicides effectively controlled *M. javanica* and *M. enterolobii*, they were less consistent against *M. incognita* in greenhouse conditions. Notably, their field trials revealed that microbial agents, including *Bacillus velezensis* (Ag109®), *B. amyloliquefaciens* (Veraneio®), *Pochonia chlamydosporia* (Rizotec®), and *Purpureocillium lilacinum* (Nemat®), only achieved nematode reduction (56.70–77.29%) when combined with the resistant rootstock 'Woodstock'.

The present study aimed to evaluate an integrated management strategy against *M.* incognita in greenhouse-grown tomato 'Apache F_1'. This approach synergizes the biological control potential of *Sporosarcina psychrophila* Sd4-11 and *Streptomyces scabiei* Wb1n-4, previously identified as effective RKN-suppressive agents in Egyptian soils (Mahmoud et al. 2025a), with grafting onto the commercial rootstocks 'Estamino' and 'Fortamino', selected for their demonstrated efficacy in RKN suppression and high productivity (Mahmoud et al. 2025b)

Materials and methods

The experiment was conducted during the 2022 and 2023 fall seasons in a naturally RKN-infested semicircular greenhouse (9 × 60 m, 3.2 m apex height) located at Monsha'et El Kanater, Giza Governorate, Egypt (30°14'44.7" N; 30°46'05.2" E). The greenhouse was covered with 150-µm-thick UV-resistant polyethylene from mid-October to early March to ensure suitable thermal conditions for tomato cultivation. Due to the absence of in situ sensors, climatic data, including monthly mean minimum and maximum air temperatures, relative humidity, and cloud cover, for the cultivation period were obtained from the NASA POWER database (https://power.larc.nasa.gov/data-access-viewer/). Internal greenhouse thermal profiles during the polyethylene-covering period were estimated using the regional calibration model of Eissa et al. (1996), which accounts for a 5–10 °C thermal gain above ambient temperatures.

Nematode diagnostics

The species identity and initial population density (*Pi*) of RKN within the experimental greenhouse were determined through soil sampling at the beginning of each experimental season prior to transplanting. For each greenhouse bed, a composite soil sample was prepared by pooling four soil cores collected at a depth of 5–30 cm using a soil auger. From each thoroughly homogenized composite sample, a 100 g subsample of fresh soil was processed using the modified Baermann funnel technique (Ayoub, 1980). To determine *Pi*, the soil subsample was placed on a double layer of cellulose tissue supported by a sieve and submerged in a water-filled funnel for 48 h at room temperature (25 ± 2 °C) to allow active nematode migration. After incubation, the nematode suspension was collected from the funnel stem, and second-stage juveniles (J_2) were counted under a stereomicroscope at 40× magnification. The Pi was expressed as the number of J_2 100 g^{-1} of soil. Simultaneously, nematode species identity was confirmed by the morphological examination of female perineal patterns ($n = 20$ female ped^{-1}) according to the diagnostic keys of Taylor and Netscher (1974).

Plant Materials

The commercial tomato rootstocks 'Estamino' (R_1) and 'Fortamino' (R_2), both characterized by the *Mi*−1/*mi*−1 genotype, were selected for grafting with the susceptible scion 'Apache F_1' (*mi*−1/*mi*−1). These rootstocks were chosen for their validated resistance to RKN and their documented capacity to enhance vegetative growth, total yield, and fruit quality (Mahmoud et al. 2025b). The cultivar 'Apache F_1' was utilized as a standard susceptible control due to its lack of the functional *Mi*−1 resistance gene, providing a critical reference point for evaluating host responses and the relative efficacy of the integrated treatments (Mahmoud et al. 2025b).

Bacterial bioagents

The bacterial isolates *Sporosarcina psychrophile* Sd4-11 (B_1) and *Streptomyces scabiei* Wb1n-4 (B_2), originally isolated and molecularly characterized by Köberl et al. (2013) from RKN-suppressive Egyptian soils, were used in this study. These isolates were selected based on their previously validated growth-promoting and nematocidal efficacy (Mahmoud et al. 2025a). To prepare pure and metabolically

active cultures, the isolates were cultured on Luria-Bertani (LB) agar in 9 cm diameter Petri dishes at 27 ± 3 °C under a 16/8 h light-dark cycle for three days until confluent growth was achieved, ensuring high metabolic activity at the time of inoculation.

Experimental procedure

Seeds of the rootstocks and scion were surface-sterilized in 2% sodium hypochlorite for 10 min, rinsed thoroughly, and dried under sterile conditions. For seed coating, fifty seeds per Petri dish were rolled over bacterial lawns of the antagonistic isolates until the seed surfaces were uniformly and completely coated. This coating methods ensured a uniform inoculum load of approximately 10^7 CFU $seed^{-1}$ as per Adam et al. (2014). Coated seeds were then air-dried under aseptic condition for 2 h prior to planting. Both coated and uncoated seeds were used to raise grafted and ungrafted plants. Seeds were sown on September 1 st of the 2022 and 2023 seasons in 209-cell trays filled with a 1:1 mixture of coconut peat and vermiculite, supplemented with nutrients. To avoid cross-contamination, two empty rows were left between treatments. Seedlings were grown in a greenhouse at 26 ± 2 °C and manually grafted at the 3–4 true-leaf stage using the slant-cut method. Grafted seedlings were placed in a high-humidity healing chamber (28 ± 2 °C, > 95% RH) for three days, gradually acclimated, and transferred to an adaptation greenhouse after one week. In mid-September, coated and uncoated grafted and ungrafted transplants were transplanted in a plastic house under a randomized complete factorial block design (RCBD) with two factors: grafting (G-R_1, G-R_2, and ungrafted: UG) seed-coating (C-B_1, C-B_2, and uncoated: UC). The experiment consisted of four replicates with 10 plants per experimental unit (EU). Pesticides were not applied, and standard greenhouse practices were followed, including fertigation with 105.8 N, 24.9 P_2O_5, 88.1 K_2O, and 10 CaO kg ha^{-1}.

Evaluated plant traits

Host RKN-responses

Host response to RKN was defined as the ability to suppress nematode development or reproduction compared to the susceptible control, 'Apache F_1' (Banora and Almaghrabi 2019). In each EU, all tomato plants were evaluated for RKN resistance by quantifying the number of galls (NG) and egg masses (NEM) produced by *M. incognita* on the root systems at the end of the fruiting season (approximately 180 DAT).

Roots were gently washed to remove adhering soil, and fresh root weights were recorded. Egg masses were visualized by staining the roots with a 0.4% cochineal red solution for 15 min (Hooper et al. 2005). After excess stain was removed by rinsing with tap water, the total number of galls and egg masses was recorded. Host responses to RKN were quantified using the Gall Index (GI; Taylor and Sasser 1978) and Egg-mass Index (EMI; Taylor 1967) on a 0–5 scale, where: 0 = no galls/egg masses (immune); 1 = 1–2 (highly resistant); 2 = 3–10 (resistant); 3 = 11–30 (moderately resistant); 4 = 31–100 (susceptible); and 5 = > 100 (highly susceptible).

Vegetative growth and morphodynamics

Morphological parameters were recorded from five representative plants per EU. Vegetative growth was evaluated at 30 and 60 days after transplanting (DAT) by measuring stem length (SL), stem diameter (SD), the number of plant leaves (NPL), and the leaf area (LA). SL was measured from the soil surface (for ungrafted plants) or the graft union (for grafted plants) to the terminal bud. SD was recorded about 1 cm above the soil surface or graft union, respectively (Mahmoud 2020). LA was determined for the fifth fully expanded leaf from the apex using the leaf-weighing technique (Pandey and Singh 2011). To quantify growth dynamics, the stem elongation rate (SER), stem thickness rate (STR), leaf formation rate (LFR), and leaf expansion rate (LER) were calculated between the two measurement intervals (30 and 60 DAT) according to Mahmoud et al. (2025b).

Reproductive development and yield components

Reproductive development was monitored by recording the number of days to the first flower anthesis (DFFE) and days to the ripening of the first ripe fruit (DFRFE) to assess treatment effects on earliness. Yield components included the number of flowers/inflorescence (NFI) and the number of fruits/cluster (NFC), both recorded from the second through the sixth clusters, and fruit set percentage (FSP). Productivity was categorized as early yield (EY), total yield (TY), and marketable yield (MY). EY was determined by the cumulative weight ofthe first three harvests, while TY comprised the total weight of all harvested fruits. MY was derived from TY after excluding defective fruits or those weighing less than 30 g (Mahmoud 2020).

Fruit quality

Fruit quality was evaluated at peak harvest using a representative sample of 20 fully red-ripe fruits per EU (Mahmoud 2020). Physical attributes included average fruit weight (AFW) and fruit firmness (FF), with the latter determined

using a Mark-10 Force Gauge (Model M4-200, Series 4). Chemical parameters consisted of pH, fruit dry matter content (FDM), total soluble solids (TSS), and vitamin C (VC). FDM was determined by oven-drying at 70 °C until constant weight was achieved. TSS was measured using a digital refractometer (PR101, Palette Co. Ltd., Tokyo, Japan), and pH was recorded bia a digital pH meter (HI 9219, Hanna Instruments, Smithfield, RI, USA). Finally, VC (ascorbic acid) concentration was quantified through titration with 2,6 dichlorophenol indophenol dye (Latimer 2012).

Photosynthetic pigments and biomass accumulation

Foliar photosynthetic pigments, i.e., chlorophyll a (Chlor-a), chlorophyll b (Chlor-b), and total carotenoids (T-Carot), were measured at 60 DAT. Pigments were extracted from 0.5 g of fresh leaf tissue in 5 ml of dimethylformamide, and concentrations were determined spectrophotometrically at 664, 647, and 480 nm following Moran (1982).

At the end of the fruiting period, 100 g of fresh shoot and root tissues were oven-dried at 70 °C to determine shoot (SDM) and root (RDM) dry matter content. Root carbohydrates (RC), proteins (RPr), and polyphenols (RPPh) were estimated using the AOAC method (Latimer 2012).

Statistical Analysis

Data normality was verified using the Shapiro-Wilk test. Variables that significantly deviated from a normal distribution ($P<0.05$) were subjected to arcsine square root transformation to satisfy ANOVA assumptions (Wickens and Keppek 2004). Data were initially subjected to a combined ANOVA across both seasons to evaluate the significance of the year factor and its interaction with experimental factors. Because significant year-to-year and interactions for several variables, each season was subsequently analyzed separately. Mean comparisons were performed using Duncan's multiple range test. MSTATc v.2.1 software (Michigan State University, Michigan, USA) was used to perform these analyses.

Principal component analysis (PCA) was performed on the standardized dataset (Z-scores) to evaluate the variability among treatments and their influence on measured traits across both experimental seasons. To ensure robust factor extraction, PCA with Varimax rotation was applied, and components were retained based on the latent root criterion (eigenvalues > 1.0; Johnson and Wichern 2007). Trait correlations and treatment clusters were visualized using PCA biplot of the first two principal components (Yan and Kang 2003). Correlation strength and direction were interpreted using the cosine of the angle between vectors: angles < 90° indicated positive correlations, > 90° indicated negative correlations, and 90° indicated no correlation. Additionally, Pearson's correlation coefficients were calculated to quantify the linear relationships between suppress *M. incognita* development indices and other morphological, physiological, and biochemicals traits. Multivariate analyses were executed using the IBM SPSS software version 26.0.0 (SPSS Inc., Chicago, Illinois, USA) and XLSTAT software version 2019 (Addinsoft, Paris, France).

Results

Nematode diagnostics

Morphological examination of female perineal patterns confirmed the identity of the nematode population as *M. incognita* (Kofoid and White) Chtwood. Observed patterns consistently displayed the diagnostic high, squarish dorsal arch and wavy cuticular striae lacking distinct lateral incisures. The morphological identification of *M. incognita* via the female perineal pattern is characterized by a high, squarish dorsal arch composed of closely spaced, smooth to wavy cuticular striae. Unlike M. javanica, this species typically lacks distinct lateral incisures (lines); instead, the striae often fork, break, or intermingle at the lateral fields, creating an indistinct boundary between the dorsal and ventral sections. The overall configuration is generally oval to pyriform, often featuring an "inverted-V" or fingerprint-like whorl immediately above the tail terminus. These diagnostic features, as established by Taylor and Netscher (1974), distinguish it from the rounded arches of *M. hapla* and the clearly divided lateral fields of *M. javanica*.

The initial population density (*Pi*) in the greenhouse topsoil (5–30 cm) was 1325 ± 105 J_2 100 g^{-1} soil during the 2022 season and 1503 ± 96 J_2 100 g^{-1} soil during the 2023 season. These values indicate that a high inoculum pressure was maintained throughout both experimental cycles, providing a robust baseline to evaluate the suppressive effects of host plant resistance compared to the susceptible control 'Apache F_1'.

Tomato phenotypes under RKN infection

ANOVA

Preliminary assessment using the Shapiro–Wilk test indicated that several parameters, including NG, NEM, SD60, NPL60, STR, SFW, SDW, RFW, RDW, DFFE, NFI, NFC, FSP, EY, TY, MY, FDM, chlor-a, RDM, RC, and RPr, significantly deviated from a normal distribution ($P<0.05$) in both growing seasons. Additional deviations were observed in season-specific variables, namely SL30, SD30, SDM,

DFRFE, chlor-b, and VC in the 2022 season, and SL60, NPL30, RPPh, pH, and TSS in the 2020 season. To ensure the validity of parametric testing, these variables were normalized using an arcsine square-root transformation prior to conducting the ANOVA. The transformed data satisfied the assumptions of normality and homogeneity of variance, thereby permitting accurate and reliable mean comparisons.

The ANOVA results for both the pooled and individual seasonal datasets for all measured phenotypic variables are presented in Table S1. The pooled ANOVA revealed that the primary experimental factors, year (Y), grafting–rootstock (GR), and seed-coating bioagents (SCB), exerted statistically significant effects on the majority of evaluated traits (Table S1). Specifically, GR significantly influenced most parameters ($P<0.01$ or 0.001), with the exceptions of STR, LFR, and pH (Table S1). Similarly, SCB significantly affected most traits ($P<0.01$ or 0.001), except for SD30, STR, LFR, and RDM (Table S1). Highly significant Y effects were observed for 35 of the 40 evaluated traits ($P<0.001$). Regarding interaction effects, the GR×SCB interaction was significant ($P<0.05$, 0.01, or 0.001) for all assessed traits except RDM (Table S1), providing strong statistical evidence for synergistic effects between these factors. Seasonal interactions were also prevalent, with significant Y×GR interactions ($P<0.05$, 0.01, or 0.001) for 24 traits, Y×SCB interactions ($P<0.05$, 0.01, or 0.001) for 28 traits, and significant three-way interactions (Y×GR×SCB; $P<0.05$, 0.01, or 0.001) for 21 traits (Table S1). Collectively, these findings underscore the dominant role of year-to-year variation, together with the robust synergistic contributions of GR and SCB, in shaping plant performance. Consequently, due to the high frequency of significant seasonal interactions, data from each growing season were analyzed separately to ensure accurate comparisons of treatment means. Seasonal ANOVA results and subsequent mean comparisons for each variable are reported separately to account for temporal variation. To quantify the magnitude of the effect of each experimental factor on the measured parameters, the percentage of the sum of squares (SS%) attributable to each factor relative to the total variation was estimated.

Host RKN-responses

Highly significant effects ($P<0.001$) of GR, SCB, and their interaction (GR×SCB) were observed on host plant RKN-responses, as quantified by NG and NEM across both seasons (Table S1). Based on SS%, SCB exerted the greatest effect on both parameters (≈36–40%), followed by the GR×SCB interaction (≈33–36%), while GR alone provided the smallest relative contribution (≈25–28%; Table S1).

Host RKN-responses are further detailed in Fig. 1. In both seasons, UG plants consistently recorded the highest NG (149.2 in 2022 and 171.4 in 2023, Fig. 1A) and NEM (163.8 in 2022 and 203.7 in 2023; Fig. 1B). Conversely, G-R_1 plants consistently exhibited the lowest NG (64.5 and 69.6, respectively; Fig. 1A) and NEM (76.8 in 2022 and 87.3 in 2023, Fig. 1B). Regarding SCB treatments, UC plants consistently showed the highest NG (162.8 in 2022 and 171.4 in 2023; Fig. 1A) and NEM (175.4 in 2022 and 212.9 in 2023, Fig. 1B). Notably, C-B_1 plants consistently recorded the lowest NG (62.7 in 2022 and 65.7 in 2023, Fig. 1A) and NEM (77.6 in 2022 and 90.9 in 2023, Fig. 1B), with a significant similarity ($P<0.05$) to C-B_2 plants for NG in 2023 (70.4) and for NEM in both seasons (79.3 in 2022 and 86.8 in 2023). UG/UC plants consistently exhibited the highest NG (302.2 in 2022 and 359.0 in 2023; Fig. 1A) and NEM (310.9 in 2022 and 404.9 in 2023, Fig. 1B). Conversely, G-R_1/C-B_1 plants consistently recorded the lowest NG (50.6 in 2022 and 55.1 in 2023, Fig. 1A) and NEM (62.0 in 2022 and 79.3 in 2023, Fig. 1B), with significant similarities ($P<0.05$) to G-R_1/C-B_2 and G-R_2/C-B_1 for NG in 2023 (57.2 and 69.5, respectively; Fig. 1A), and to G-R_1/C-B_2

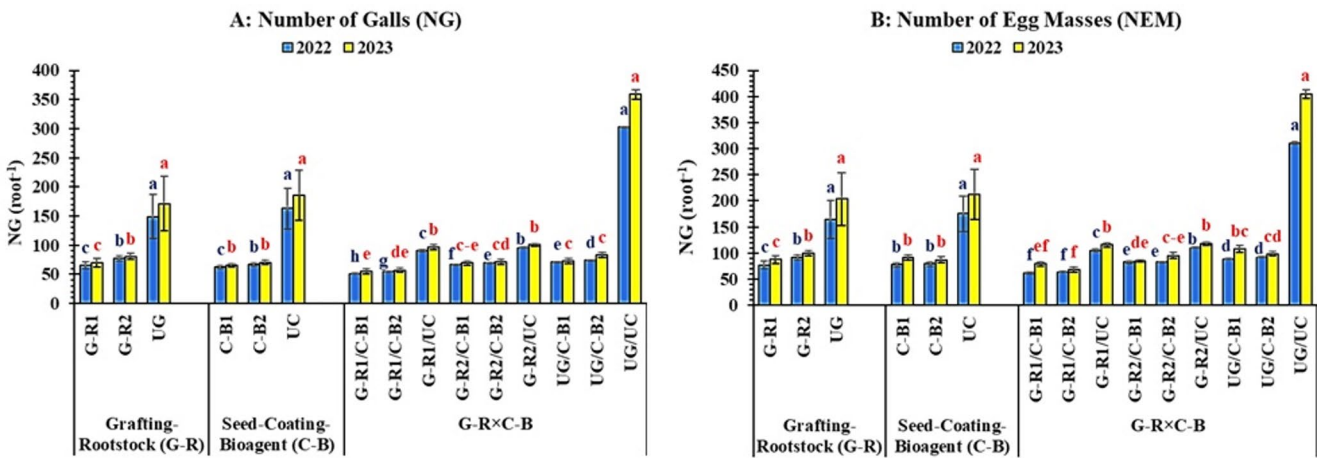

Fig. 1 Effects of grafting and bioagent seed coating on galling (A) and egg masses (B) of *Meloidogyne incognita* in tomato 'Apache F_1'

for NEM in both seasons (63.4 in 2022 and 67.4 in 2023, Fig. 1B).

Stem and leaf morphogenesis

Highly significant effects ($P<0.001$) of GR, SCB, and their interaction were observed on stem length (cm) at 30 (SL30) and 60 DAT (SL60) during both seasons (Table S1). GR exerted the greatest influence on stem elongation, contributing the highest SS% for SL30 (61.1 in 2022 and 40.9 in 2023) and SL60 (54.1 in 2022 and 57.3 in 2023). The subsequent relative contributions were to SCB (SS% for SL30: 14.0 in 2022 and 43.8 in 2023; SS% for SL60: 27.4 in 2022 and 20.8 in 2023) and the interaction (SS% for SL30: 20.8 in 2022 and 8.2 in 2023; SS% for SL60: 11.2 in 2022 and 11.9 in 2023), with their relative contributions varying between seasons (Table S1).

Stem morphogenesis traits for grafted and ungrafted 'Apache F_1' plants, with or without bioagent-based seed-coating, are presented in Fig. 2. G-R_1 plants consistently exhibited the greatest SL30 (66.3 in 2022 and 79.4 in 2023; Fig. 2A) and SL60 (107.0 in 2022 and 118.6 in 2023; Fig. 2B) and were significantly similar ($P<0.05$) to G-R_2 for SL30 in 2023 (79.6; Fig. 2A). In contrast, UG plants consistently produced the lowest SL30 (55.9 in 2022 and 66.8 in 2023; Fig. 2A) and SL60 (86.33 in 2022 and 88.4 in 2023; Fig. 2B). Among the SCB treatments, C-B_1 consistently recorded the maximum SL30 (64.8 in 2022 and 83.4 in 2023; Fig. 2A) and SL60 (103.9 in 2022 and 110.6 in 2023; Fig. 2B) and was significantly similar ($P<0.05$) to C-B_2 for SL60 in 2023 (109.4; Fig. 2B). Conversely, UC plants exhibited the minimum SL30 (59.7 in 2022 and 68.4 in 2023; Fig. 2A) and SL60 (89.3 in 2022 and 95.0 in 2023; Fig. 2B). Combined treatment G-R_1/C-B_1 consistently produced the greatest SL30 (69.3 in 2022 and 89.5

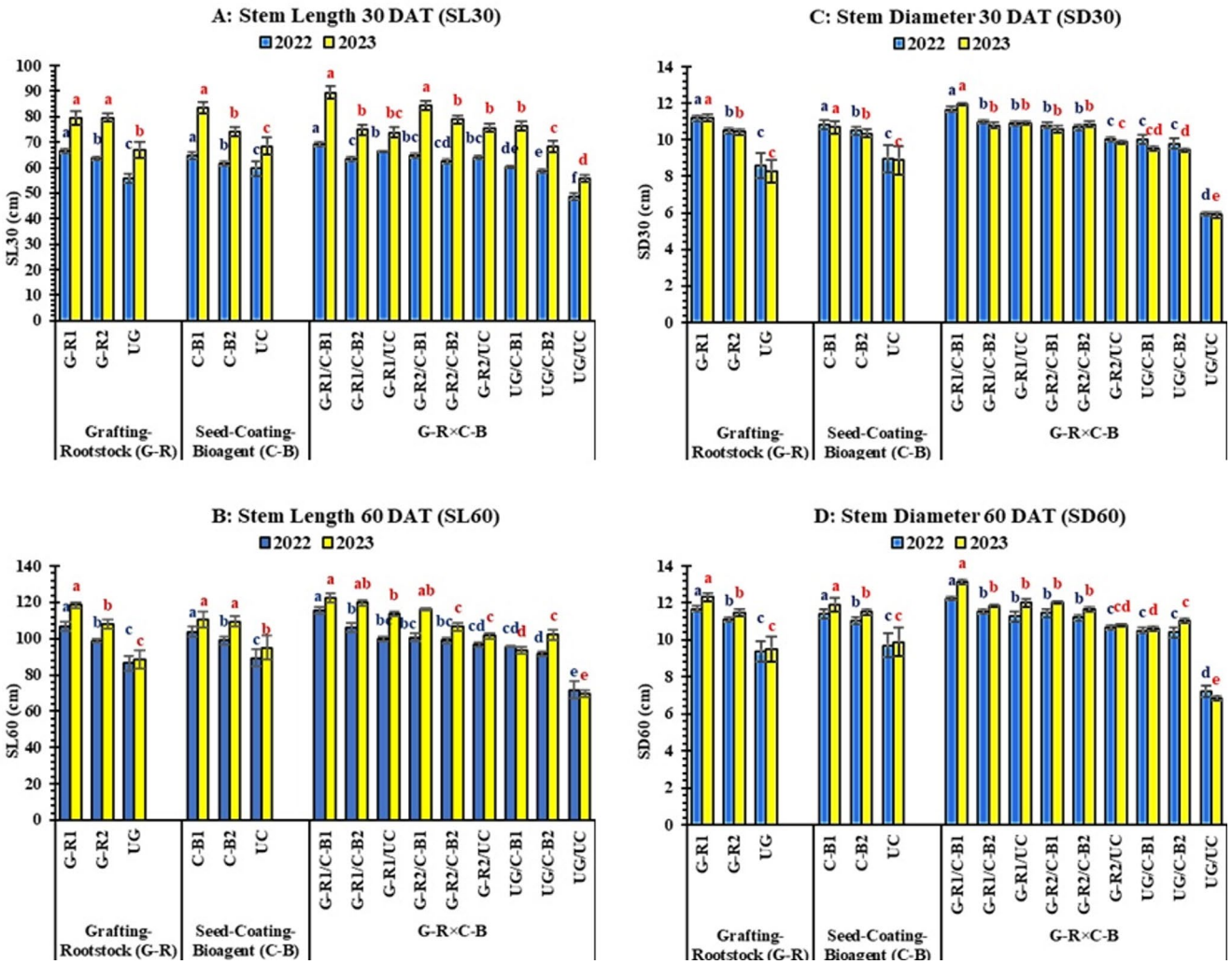

Fig. 2 Effects of grafting and bioagent seed coating on tomato 'Apache F_1' stem morphogenesis under *Meloidogyne incognita* infestation. A-B: stem length at 30 and 60 DAT, respectively, and D-E: stem diameter at 30 and 60 DAT, respectively

in 2023; Fig. 2A) and SL60 (115.3 in 2022 and 122.3 in 2023; Fig. 2B), showing significant similarity ($P<0.05$) to G-R_2/C-B_1 for SL30 and SL60 in 2023 (84.4 and 116.2, respectively) and to G-R_1/C-B_2 for SL60 in 2023 (119.6). Conversely, the UG/UC combination consistently produced the lowest SL30 (48.7 in 2022 and 55.7 in 2023; Fig. 2A) and SL60 (71.7 in 2022 and 69.6 in 2023; Fig. 2B).

Stem diameter (SD, mm) at both 30 (SD30) and 60 DAT (SD60) was highly significantly influenced ($P<0.001$) by GR, SCB, and their interaction across both seasons (Table S1). GR contributed the largest SS% for SD30 (48.33 in 2022 and 57.51 in 2023) and SD60 (50.24 in 2022 and 57.51 in 2023), followed by SCB (SS% for SD30: 26.50 in 2022 and 22.78 in 2023; SS% for SD60: 27.45 in 2022 and 27.31 in 2023), and their interaction (SS% for SD30: 23.01 in 2022 and 18.60 in 2023; SS% for SD60: 18.01 in 2022 and 21.48 in 2023), with seasonal differences in relative contribution (Table S1). G-R_1 plants consistently exhibited the maximum SD30 (11.18 in 2022 and 11.21 in 2023; Fig. 2C) and SD60 (11.68 in 2022 and 12.32 in 2023; Fig. 2D), while UG plants developed lowest SD30 (8.59 in 2022 and 8.28 in 2023; Fig. 2C) and SD60 (9.37 in 2022 and 9.50 in 2023; Fig. 2D). Among SCB treatments, C-B_1 produced the widest SD30 (10.82 in 2022 and 10.68 in 2023; Fig. 2C) and SD60 (11.40 in 2022 and 11.91 in 2023; Fig. 2D), while UC plants exhibited thinner SD30 (8.96 in 2022 and 8.89 in 2023; Fig. 2C) and SD60 (9.71 in 2022 and 9.89 in 2023; Fig. 2D). The combined treatment G-R_1/C-B_1 consistently produced the greatest SD30 (11.67 in 2022 and 11.94 in 2023; Fig. 2C) and SD60 (12.23 in 2022 and 13.13 in 2023; Fig. 2D), whereas the UG/UC combination consistently exhibited the minimum SD30 (5.97 in 2022 and 5.89 in 2023; Fig. 2C) and SD60 (7.20 in 2022 and 6.86 in 2023; Fig. 2D).

The number of plant leaves (NPL) at 30 (NPL30) and 60 DAT (60DAT) was highly significantly affected ($P<0.01$ or 0.001) by GR, SCB, and their interaction across both seasons (Table S1). GR exerted the strongest influence on both traits (SS% for NPL30: 64.83 in 2022 and 55.95 in 2023; SS% for NPL60: 61.71 in 2022 and 48.57 in 2023), followed by GR×SCB interaction (SS% for NPL30: 10.79 in 2022 and 22.08 in 2023; SS% for NPL60: 14.06 in 2022 and 30.21 in 2023), and SCB (SS% for NPL30: 8.56 in 2022 and 18.03 in 2023; SS% for NPL60: 11.71 in 2022 and 12.24 in 2023; Table S1).

Leaf morphogenesis traits for grafted and ungrafted 'Apache F_1' plants, with or without bioagent-based seed-coating, are presented in Fig. 2. G-R_1 plants consistently produced the maximum NPL30 (9.67 in 2022 and 10.29 in 2023; Fig. 3A) and NPL60 (13.95 in 2022 and 12.24 in 2023; Fig. 3B), whereas UG plants consistently produced the fewest NPL30 (6.67 in 2022 and 7.65 in 2023; Fig. 3A) and NPL60 (10.33 in 2022 and 10.26 in 2023; Fig. 3B). Among seed coating treatments, C-B_1 consistently produced the highest NPL30 (8.89 in 2022 and 9.91 in 2023; Fig. 3A) and NPL60 (13.15 in 2022 and 11.74 in 2023; Fig. B), showing significant similarity ($P<0.05$) to C-B_2 for SL60 in both seasons (12.48 in 2022 and 11.61 in 2023; Fig. 3B). Conversely, UC plants consistently showed the minimum NPL30 (7.89 in 2022 and 8.40 in 2023; Fig. 3A) and NPL60 (11.54 in 2022 and 10.80 in 2023; Fig. 3B). The combined treatment G-R_1/C-B_1 produced the greatest NPL30 (10.0 in 2022 and 10.8 in 2023; Fig. 3A) and NPL60 (14.49 in 2022 and 12.05 in 2023; Fig. 3B), showing significant similarity ($P<0.05$) to G-R_1/C-B_2, G-R_1/UC, and G-R_2/C-B_1 for NPL30 in 2022 (ranging 9.0 to 10.0; Fig. 3A) and for NPL60 in both seasons (ranging 13.82–13.70 in 2022 and 11.70–12.45.70.45 in 2023; Fig. 3B); to G-R_2/UC for NPL30 in 2022 (8.67; Fig. 3A); and to G-R_2/C-B_2 for NPL60 (11.71; Fig. 3B). Conversely, the UG/UC combination consistently exhibited the lowest NPL30 (5.33 in 2022 and 5.62 in 2023; Fig. 3A) and NPL60 (8.05 in 2022 and 8.40 in 2023; Fig. 3B).

Leaf area (cm^2) at 30 (LA30) and 60 DAT (LA60) was highly significantly influenced ($P<0.001$) by GR, SCB, and their interaction in both seasons, except for the interaction on LA30 in 2023 (Table S1). GR consistently exerted the strongest effect on both traits in both seasons (SS% for LA30: 60.52 in 2022 and 64.74 in 2023; SS% for LA60: 54.27 in 2022 and 55.39 in 2023), followed by GR×SCB interaction (SS% for LA30: 31.02 in 2022 and 21.63 in 2023; SS% for LA60: 34.57 in 2022 and 28.95 in 2023), then SCB (SS% for LA30: 4.48 in 2022 and 3.63 in 2023; SS% for LA60: 7.81 in 2022 and 10.85 in 2023; Table S1). Across seasons, G-R_1 plants consistently achieved the maximum LA30 (211.15 in 202 and 211.82 in 2023; Fig. 3C) and LA60 (222.63 in 2022 and 230.04 in 2023; Fig. 3D), with a significant similarity ($P<0.05$) to G-R_2 for LA30 and LA60 in 2023 (208.16 and 221.94, respectively). Conversely, UG plants consistently exhibited the lowest LA30: 185.83 in 2022 and 194.14 in 2023; Fig. 3C) and LA60 (199.55 in 2022 and 211.11 in 2023; Fig. 3D). Among SCB treatments, C-B_1 consistently produced the greatest LA30 (209.17 in 2022 and 207.94 in 2023; Fig. 3C) and LA60 (221.92 in 2022 and 227.79 in 2023; Fig. 3D). In contrast, UC plants showed the smallest LA30 (195.58 in 2022 and 198.48 in 2023), significantly similar ($P<0.05$) to C-B_2 in 2022 (192.11; Fig. 3C). For LA60, the minimum value was recorded in C-B_2 in 2022 (204.54) and UC in 2023 (214.06; Fig. 3D). The combined treatment G-R_1/C-B_1 consistently produced the largest LA30 (226.63 in 2022 and 216.74 in 2023; Fig. 3C) and LA60 (239.50 in 2022 and 241.0 in 2023; Fig. 3D), with a significant similarity ($P<0.05$) to G-R_1/C-B_2 for LA30 in 2023 (213.34). In contrast, UG/UC consistently recorded the lowest LA30 (181.98 in 2022

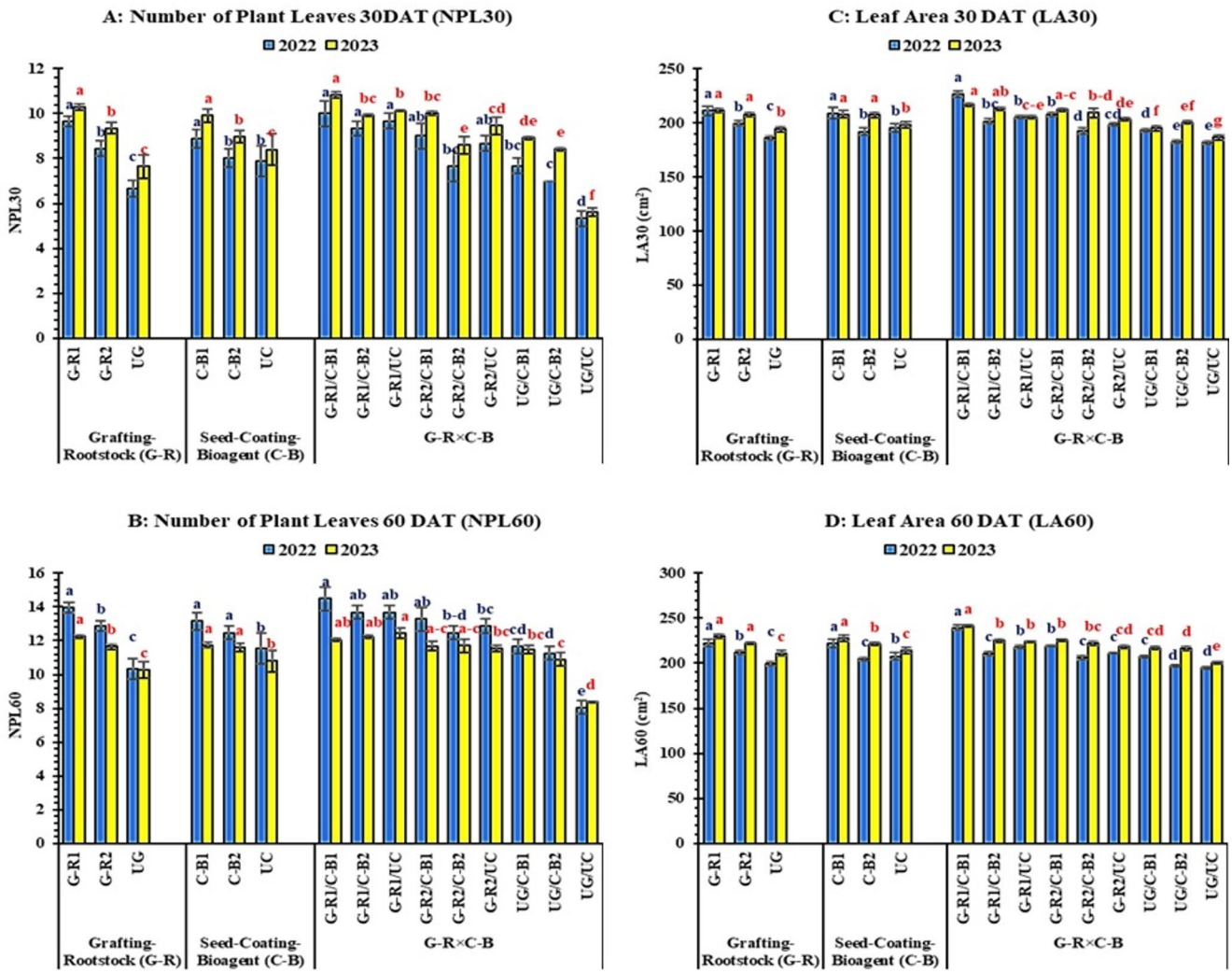

Fig. 3 Effects of grafting and bioagent seed coating on tomato 'Apache F_1' leaf morphogenesis under *Meloidogyne incognita* infestation. A-B: number of plant leaves at 30 and 60 DAT, respectively, and D-E: leaf area at 30 and 60 DAT, respectively

and 186.84 in 2023; Fig. 3C) and LA60 (194.86 in 2022 and 200.11 in 2023; Fig. 3D), with significant similarities ($P<0.05$) to UG/C-B_2 for LA30 and LA60 in 2022 (182.35 and 196.78, respectively).

Stem and leaf morph-dynamics

Stem and leaf morph-dynamics for grafted and ungrafted 'Apache F_1' plants, with or without bioagent-based seed-coating, are presented in Fig. 4.

Stem elongation rate (SER; cm day^{-1}) was highly significantly affected ($P<0.001$) by GR, SCB, and their interaction in both seasons, except for the interaction in 2022 (Table S1). GR exerted the strongest influence on SER (SS%: 38.1 in 2022 and 57.3 in 2023), followed by either SCB (SS%: 36.7 in 2022 and 17.8 in 2023) or the interaction (SS%: 6.9 in 2022 and 20.8 in 2023), depending on the season (Table S1). G-R_1 plants consistently achieved the maximum SER (1.36 in 2022 and 1.31 in 2023), whereas UG plants showed the minimum values (1.01 in 2022 and 0.72 in 2023) (Fig. 4A). Among seed-coating treatments, C-B_2 recorded the highest SER (1.25 in 2022 and 1.18 in 2023), significantly similar ($P<0.05$) to C-B_1 in 2022 (1.30; Fig. 4A). Conversely, UC plants exhibited the lowest SER (0.99 in 2022 and 0.89 in 2023), being significantly similar ($P<0.05$) to C-B_1 in 2023 (0.91; Fig. 4A). The combined treatment G-R_1/C-B_2 consistently produced the greatest SER (1.42 in 2022 and 1.50 in 2023), significantly similar ($P<0.05$) to G-R_1/C-B_1 in 2022 (1.53; Fig. 4A). Conversely, the UG/UC combination consistently showed the lowest SER (0.77 in 2022 and 0.46 in 2023), significantly similar ($P<0.05$) to UG/C-B_1 in 2023 (0.57) (Fig. 4A).

Only stem thickness rate (STR: mm day^{-1}) was significantly affected ($P<0.01$ and 0.05) by the GR×SCB interaction in both seasons (Table S1). The combined treatment UG/UC consistently exhibited the highest STR (0.041

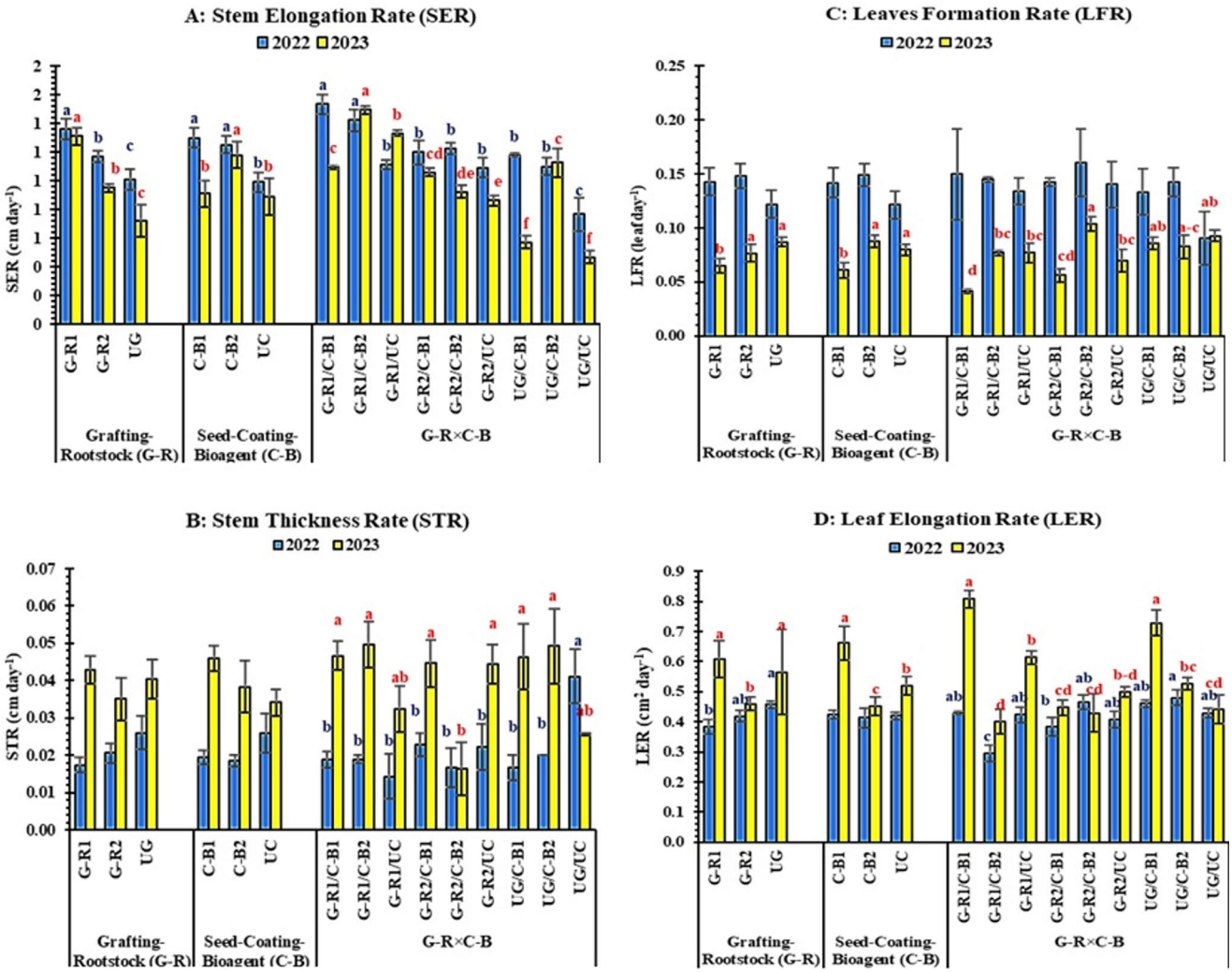

Fig. 4 Effects of grafting and bioagent seed coating on stem and leaf morpho-dynamics of tomato 'Apache F_1' under *Meloidogyne incognita* infestation. A: stem elongation rate; B: stem thickness rate, C: leaves formation rate, and D: leaf elongation rate

in 2022 and 0.026 in 2023), with significant similarities ($P<0.05$) to the other treated plants in 2023 (ranging 0.03–0.05; Fig. 4B).

Leaf formation rate (LFR; leaf day^{-1}) was significantly affected ($P<0.001$) by GR, SCB, and the GR×SCB interaction in 2023 only (Table S1). G-R_2 and UG plants showed the highest LFR (0.08 and 0.09, respectively), with significant similarities ($P<0.05$) among them, whereas G-R_1 recorded the lowest (0.07) (Fig. 4C). Among SCB treatments, C-B_2 and UC plants had the greatest LFR (0.09 and 0.08, respectively), and C-B_1 the lowest (0.06; Fig. 4C). The combined treatments G-R_2/C-B_2, UG/C-B_1, UG/C-B_2, and UG/UC achieved the highest LFR (0.10, 0.09, 0.08, and 0.09, respectively), with significant similarities ($P<0.05$) among them (Fig. 4C). In contrast, G-R_1/C-B_1 and G-R_2/C-B_1 plants resulted in the lowest LFR (0.04 and 0.06, respectively), with significant similarity ($P<0.05$) among them (Fig. 4C). Leaf elongation rate (LER; cm^2 day^{-1}) was significantly affected by GR and GR×SCB interaction in both seasons ($P<0.01$ or 0.001), and by SCB in only 2023 ($P<0.01$; Table S1). The GR×SCB interaction consistently accounted for the largest portion of variation in LER (47.12% in 2022 and 32.26% in 2023), followed by either GR (25.17% in 2022 and 18.46% in 2023) or SCB (0.36% in 2022 and 36.56% in 2023), depending on the season (Table S1). UG plants consistently recorded the highest LER (0.46 in 2022 and 0.57 in 2023), with a significant similarity ($P<0.05$) to G-R_2 in 2022 (0.42) and G-R1 in 2023 (0.60; Fig. 4D). In 2023, C-B_1 plants had the highest LER (0.66), while C-B_2 plants had the lowest (0.45; Fig. 4D). Among combined treatments, the highest LER were observed in G-R1/C-B1 (0.43 in 2022 and 0.81 in 2023) and UG/C-B_1 (0.46 in 2022 and 0.73 in 2023), with significant similarities ($P<0.05$) among them and to G-R_1/UC, G-R_2/C-B_2, G-R_2/UC, UG/C-B_2, and UG/UC in 2022 (0.42, 0.47, 0.41, 0.48, and 0.43, respectively; Fig. 4D). Conversely, G-R_1/C-B_2 consistently

had the lowest LER (0.30 in 2022 and 0.40 in 2023), significantly similar ($P<0.05$) to G-R_2/C-B_1, G-R_2/C-B_2, G-R_2/UC, and UG/UC in 2023 (ranging 0.42–0.50; Fig. 4D).

Shoot and root fresh and dry weight

Stem and root fresh and dry weight for grafted and ungrafted 'Apache F_1' plants, with or without bioagent-based seed-coating, are presented in Fig. 5.

Shoot fresh weight (SFW; g) and shoot dry weight (SDW; g) were highly significantly influenced ($P<0.001$) by GR, SCB, and their interaction across both seasons (Table S1). The relative variance contribution (SS%) varied by season: GR contributed 27.26% and 36.51% of SFW and 25.33% and 54.00% of SDW; SCB accounted for 31.33% and 21.14% of SFW and 42.77% and 19.74% of SDW; while the GR×SCB interaction explained 41.28% and 42.22% of SFW and 29.04% and 24.42% of SDW (Table S1). G-R_1 consistently produced the highest SFW (845.7 g in 2022 and 711.8 g in 2023; Fig. 5A) and SDW (130.5 in 2022 and 107.7 in 2023; Fig. 5B), with a significant similarity ($P<0.05$) to G-R_2 in 2023 for SFW (842.8; Fig. 5A) and SDW (129.5; Fig. 5B). UG plants consistently recorded the lowest SFW (112.0 in 2022 and 82.4 in 2023; Fig. 5A) and SDW (16.3 in 2022 and 14.2 in 2023; Fig. 5B). Among SCB treatments, C-B_1 consistently achieved the highest SFW (848.9 in 2022 and 696.3 in 2023; Fig. 5A) and SDW (135.4 in 2022 and 103.6 in 2023; Fig. 4B), with a significant similarity ($P<0.05$) to C-B_2 for SFW (846.4 in 2022 and 695.3 in 2023; Fig. 5B). Conversely, UC plants consistently showed the lowest SFW (697.0 in 2022 and 603.8 in 2023; Fig. 5A) and SDW (109.1 in 2022 and 88.3 in 2023; Fig. 5B). The combined treatment UG/UC consistently recorded the lowest SFW (440.4 in 2022 and 401.1 in 2023; Fig. 5A) and SDW (79.3 in 2022 and 59.1 in 2023; Fig. 5B), while G-R_1/C-B_1 consistently produced the highest SFW (860.4 in 2022 and 714.2 in

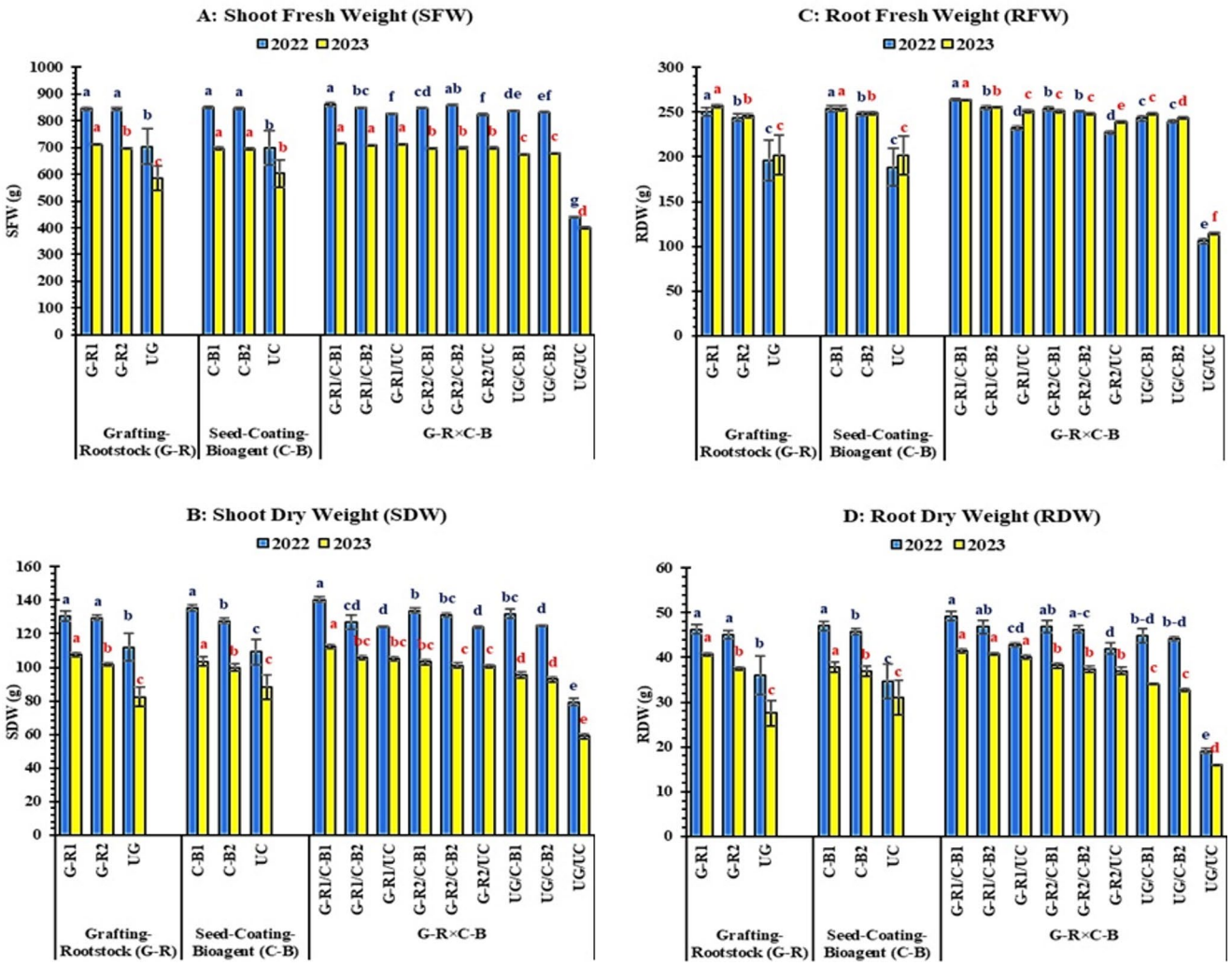

Fig. 5 Effects of grafting and bioagent seed coating on shoot and root fresh and dry weight of tomato 'Apache F_1' under *Meloidogyne incognita* infestation. A-B: fresh and dry weight of shoot, respectively, and C-D: fresh and dry weight of root, respectively

2023; Fig. 5A) and SDW (140.4 in 2022 and 112.3 in 2023; Fig. 5B), with significant similarities ($P<0.05$) to G-R_1/C-B_2 and G-R_1/UC for SFW in 2023 (708.9 and 712.2, respectively; Fig. 5A).

Root fresh (RFW; g) and dry weight (RDW; g) were highly significantly affected ($P<0.001$) by GR, SCB, and their interaction in both seasons (Table S1). The relative variance contribution (SS%) varied by season: GR explained 28.34% and 29.91% of RFW and 27.86% and 57.68% of RDW; SCB accounted for 42.54% and 30.14% of RFW and 41.31% and 16.91% of RDW; while the G×C interaction contributed 28.66% and 39.79% to RFW and 27.79% and 24.57% to RDW (Table S1). G-R_1 plants consistently exhibited the greatest RFW (250.4 in 2022 and 256.7 in 2023; Fig. 5C) and RDW (46.3 in 2022 and 40.7 in 2023; Fig. 5D), with a significant similarity ($P<0.05$) to G-R_2 for RDW in 2022 (45.1; Fig. 5D). UG plants consistently recorded the lowest RFW (196.3 in 2022 and 202.2 in 2023; Fig. 5C) and RDW (36.1 in 2022 and 27.6 in 2023; Fig. 5D). Among SCB treatments, C-B_1 consistently achieved the greatest RFW (253.8 in 2022 and 254.3 in 2023; Fig. 5C) and RDW (47.0 in 2022 and 37.9 in 2023; Fig. 5D), while UC plants consistently showed the lowest RFW (188.6 in 2022 and 201.7 in 2023; Fig. 5C) and RDW (34.6 in 2022 and 31.0 in 2023; Fig. 5D). The combined treatment UG/UC consistently recorded the lowest RFW (106.1 in 2022 and 114.5 in 2023; Fig. 5C) and RDW (19.1 in 2022 and 16.0 in 2023; Fig. 5D), while G-R_1/C-B_1 consistently produced the greatest RFW (264.1 in 2022 and 263.5 in 2023; Fig. 5C) and RDW (49.3 in 2022 and 41.4 in 2023; Fig. 5D), with significant similarities ($P<0.05$) for RDW to G-R_1/C-B_2 in both seasons (46.8 and 40.7, respectively), and to G-R_2/C-B_1 and G-R_2/C-B_2 in 2022 (47.0 and 46.3 g, respectively), and to G-R_1/UC in 2023 (40.1 g).

Reproductive development timing

Days to first flower emission (DFFE; day) and to first ripe fruit emission (DFRFE; day) were significantly influenced ($P<0.01$ or 0.001) by GR and SCB factors in both seasons, and by the GR×SCB interaction for DFFE in 2023 and for DFRFE in 2022 ($P<0.001$; Table S1). The relative contributions to variance varied by season: GR accounted for 26.62% and 31.64% of DFFE and 26.53% and 54.91% of DFRFE; SCB explained 26.28% and 25.18% of DFFE and 48.65% and 20.14% of DFRFE; while the GR×SCB interaction contributed 15.27% and 40.12% to DFFE and 24.02% and 6.06% to DFRFE (Table S1). GR explained a larger portion of the variation in DFRFE, whereas SCB had a stronger effect on DFFE.

Reproductive development timing for grafted and ungrafted 'Apache F_1' plants, with or without bioagent-based seed-coating, is presented in Fig. 6. UG plants showed significantly delayed phenological development, with higher DFFE (36.65 in 2022 and 38.59 in 2023; Fig. 6A) and DFRFE values (75.78 in 2022 and 75.10 in 2023; Fig. 6B). Conversely, G-R_1 plants flowered and fruited earlier, showing lower values of DFFE (29.25 in 2022 and 31.62 in 2023; Fig. 6A) and DFRFE (68.89 in 2022 and 69.05 in 2023; Fig. 6B), significantly similar ($P<0.05$) to G-R_2 in DFFE in both seasons (30.93 in 2022 and 32.13 in 2023) and in DFRFE in only 2023 (70.50). Among SCB treatments, UC exhibited significantly delayed phenological development, as indicated by higher DFFE (36.48 in 2022 and 38.11 in 2023; Fig. 6A) and DFRFE values (77.11 in 2022 and 72.29 in 2023; Fig. 6D), being significantly similar ($P<0.05$) to C-B_2 plants in DFRFE only in 2023 (72.98). Conversely, C-B_1 plants showed earlier flowering and fruit ripening, with lower DFFE (28.91 in 2022 and 32.22 in

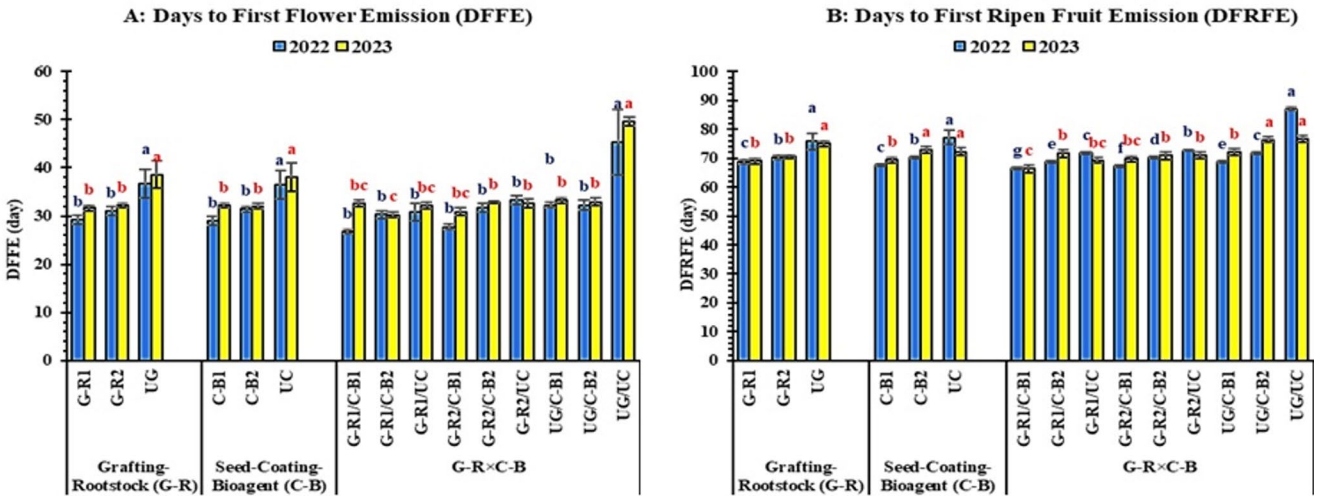

Fig. 6 Effects of grafting and bioagent seed coating on reproductive development timing of tomato 'Apache F_1' under *Meloidogyne incognita* infestation. A: days to first flower emission and B: days to first ripen fruit emission

2023; Fig. 6A) and DFRFE values (67.44 in 2022 and 69.44 in 2023; Fig. 6B), significantly similar ($P<0.05$) to C-B_2 in DFFE in both seasons (28.91 in 2022 and 32.22 in 2023). The combined treatment G-R_1/C-B_1 further enhanced earliness, resulting in the lowest DFFE (26.73 in 2022 and 32.533 in 2023; Fig. 6A) and DFRFE values (66.33 in 2022 and 66.34 in 2023; Fig. 6D), significantly similar ($P<0.05$) to G-R_1/C-B_2, G-R_1/UC, G-R_2/C-B_1 for DFFE in both seasons (ranging from 27.74 to 30.76 in 2022 and 30.10–32.11 in 2023). Conversely, UG/UC exhibited pronounced delays in phenological development, with the highest DFFE (45.39 in 2022 and 49.58 in 2023; Fig. 6A) and DFRFE values (87.00 in 2022 and 76.77 in 2023; Fig. 6B).

Yield and its components

Plant yield components (NF/I, NF/C, FSP, and AFW) were significantly affected ($P<0.01$ or 0.001) by GR, SCB, and their interaction in both seasons, although the magnitude of their effects varied by season (Table S1). In 2022, GR, SCB, and GR×SCB explained 21.31–31.44%, 24.94–60.66%, and 10.09–30.22%, respectively, of the variation, while in 2023 their contributions were 19.77–39.42%, 18.91–33.04%, and 34.45–42.28%, respectively (Table S1).

Plant yield components (NF/I, NF/C, FSP, and AFW) for grafted and ungrafted 'Apache F_1' plants, with or without bioagent-based seed-coating, are presented in Fig. 7. UG plants consistently exhibited the lowest NF/I (8.7 in 2022 and 8.8 in 2023; Fig. 7A), NF/C (6.6 in 2022 and 7.1 in 2023; Fig. 7B), FSP (72.4% in 2022 and 76.4% in 2023; Fig. 7C), and AFW (92.3 g in 2022 and 93.5 g in 2023; Fig. 7D). In contrast, G-R_1 plants consistently exhibited the highest NF/I (10.33 in 2022 and 10.35 in 2023; Fig. 7A), NF/C (9.11 in 2022 and 9.57 in 2023; Fig. 7B), FSP (87.86% in 2022 and 92.37% in 2023; Fig. 7C), and AFW (113.67 g in 2022 and 113.95 g in 2023; Fig. 7D), with G-R_2 showing significantly

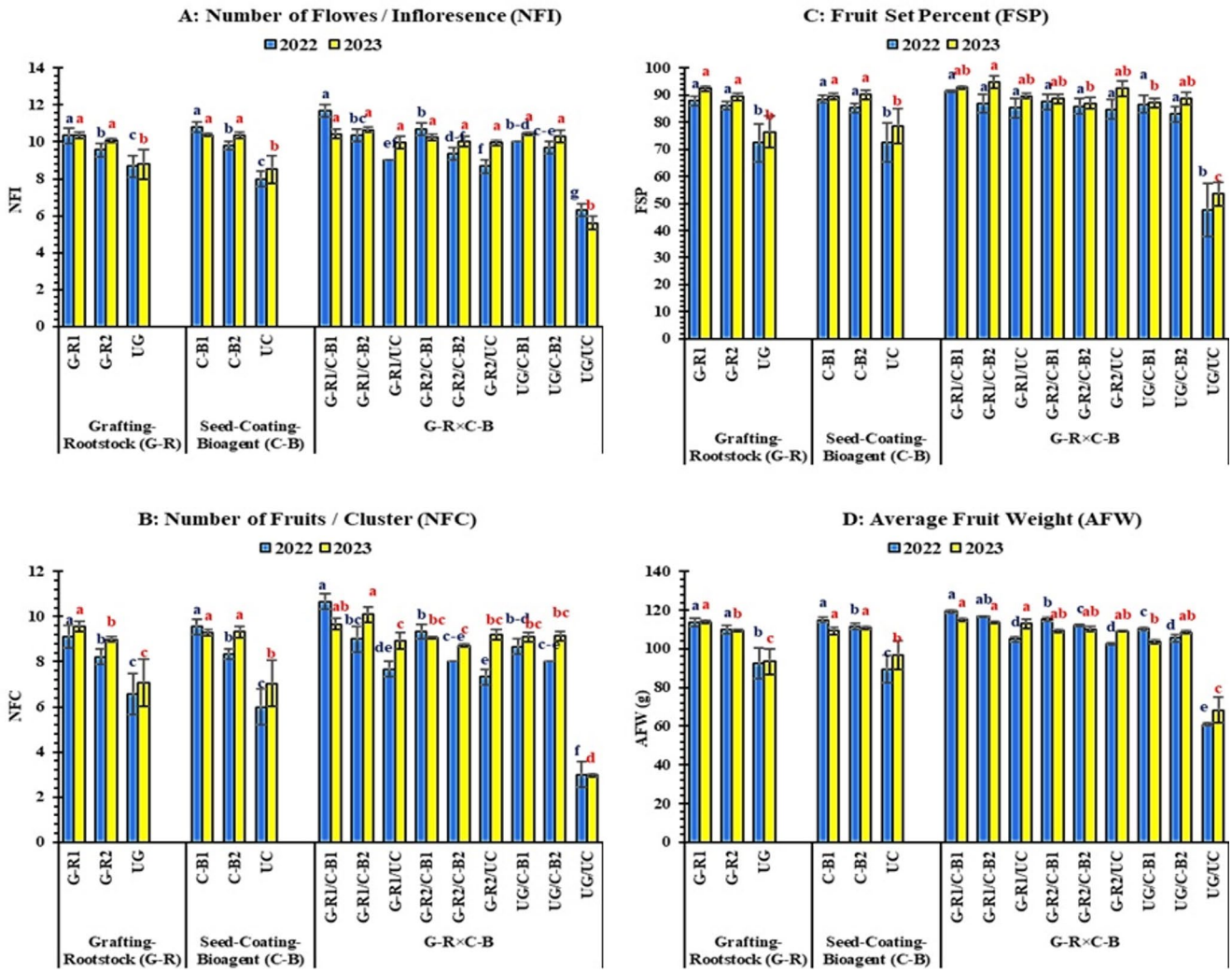

Fig. 7 Effects of grafting and bioagent seed coating on yield components of tomato 'Apache F_1' under *Meloidogyne incognita* infestation. A: number of flowers per inflorescence, B: number of fruits per cluster, C: fruit set percentage, and D: average fruit weight

similar performance ($P<0.05$) for NF/I in 2023 (10.07), FSP in both seasons (86.07% and 89.40%, respectively), and AFW in 2022 (110.00 g). Among seed-coating treatments, UC plants consistently exhibited the poorest performance for NF/I (8.00 in 2022 and 8.50 in 2023; Fig. 7A), NF/C (6.00 in 2022 and 7.03 in 2023; Fig. 7B), FSP (72.51% in 2022 and 78.551% in 2023; Fig. 7C), and AFW (89.56 g in 2022 and 96.85 g in 2023; Fig. 7D). C-B_1 plants consistently exhibited the better performance for NF/I (10.78 in 2022 and 10.37 in 2023; Fig. 7A), NF/C (9.56 in 2022 and 9.28 in 2023; Fig. 7B), FSP (88.55% in 2022 and 89.51% in 2023; Fig. 7C), and AFW (115.00 g in 2022 and 109.30 g in 2023; Fig. 7D), with C-B_2 showing significantly similar performance ($P<0.05$) in 2023 for NF/I (10.34), NF/C (9.32), and AFW (110.79 g), and in both seasons for FSP (85.29 and 90.12%, respectively). The strongest interaction effect was observed in the G-R_1/C-B_1 combination, which consistently showed the highest NF/I (11.67 in 2022 and 10.43 in 2023; Fig. 7A), NF/C (10.67 in 2022 and 9.67 in 2023; Fig. 7B), FSP (91.41% in 2022 and 92.76% IN 2023; Fig. 7C), and AFW (119.33 G IN 2022 and 115.07 in 2023; Fig. 7D), with G-R_1/C-B_2 showing significantly similar results ($P<0.05$) for some components (Fig. 7). Conversely, UG/UC plants consistently showed the lowest performance for NF/I (6.33 in 2022 and 5.61 in 2023; Fig. 7A), NF/C (3.00 in 2022 and 2.97 in 2023; Fig. 7B), FSP (47.62% in 2022 and 53.49% in 2023; Fig. 7C), and AFW (61.00 g in 2022 and 68.43 g in 2023; Fig. 7D).

Plant yields: early (EY; g), total (TY; g), and marketable (MY; g), were highly significantly affected ($P<0.001$) by GR, SCB, and their interaction in both seasons (Table S1). The GR×SCB interaction consistently explained the largest proportion of variation (≈41–45%), followed by SCB (≈29–31%), and GR (≈26–28%) (Table S1). Plant yields for grafted and ungrafted 'Apache F_1' plants, with or without bioagent-based seed-coating, are presented in Fig. 8. G-R_1 plants consistently exhibited the highest EY (778.83 in 2022 and 942.39 in 2023; Fig. 8A), TY (2402.61 in 2022 and 3003.26 in 2023; Fig. 8B), and MY (2316.02 in 2022 and 2756.06 in 2023; Fig. 8C), while UG plants showed the lowest performance (EY: 533.52 in 2022 and 645.56 in 2023; TY: 1740.35 in 2022 and 2175.43 in 2023, and MY: 1600.34 in 2022 and 1904.41 in 2023). Among SCB treatments, C-B_1 consistently provided the best performance for EY (783.05 in 2022 and 947.49 in 2023; Fig. 8A), TY (2404.28 in 2022 and 3005.36 in 2023; Fig. 8B), and MY (2313.85 in 2022 and 2753.48 in 2023; Fig. 8C), with C-B_2 showing significantly similar ($P<0.05$) MY in both seasons (2302.93 in 2022 and 2740.49 in 2023; Fig. 8C). G-R_1/C-B_1 and G-R_1/C-B_2 consistently produced the highest EY (791.78-786.22.78.22.78.22 in 2022 and 958.0-951.33.0.33.0.33 in 2023; Fig. 8A), TY (2442.36-2434.78.36.78.36.78 in 2022 and3052.95-3043.47.95.47.95.47 in 2023; Fig. 8B), and MY (2384.38-2352.5438.54.38.54 in 2022 and 2837.41-2799.52.41.52.41.52 in 2023; Fig. 8C), whereas UG/UC plants had the poorest performance EY (59.02 in 2022 and 71.41 in 2023; Fig. 8A), TY (527.75 in 2022 and 659.68 in 2023; Fig. 8B), and MY (317.54 in 2022 and 377.88 in 2023; Fig. 8C).

Fruit quality

Fruit quality traits for grafted and ungrafted 'Apache F_1' plants, with or without bioagent-based seed-coating, are presented in Fig. 9.

Fruit pH was significantly affected ($P<0.05$, 0.01, or 0.001) by GR, SCB, and their interaction, although their impacts varied (Table S1). SCB contributed for the largest proportion of variance (76.0% in 2022; 33.3% in 2023), followed by GR×SCB, particularly in 2023 (47.21%), while the GR effect remained minimal (7.14% in 2022; 6.02% in 2023) (Table S1). G-R_2 plants consistently produced the highest pH (4.24 in 2022 and 3.51 in 2023), with a significant similarity to UG in 2022 (4.41) and G-R_1 in 2023 (3.53) (Fig. 9A). Conversely, the lowest pH values were observed in G-R_1 in 2022 (4.01) and in UG in 2023 (3.38). Among the SCB treatments, the highest pH values were recorded in UC in 2022 (4.87) and C-B1 in 2023 (3.69), while the lowest values were recorded in C-B_1 in 2022 (3.56) and C-B_2 and UC in 2023 (3.34 and 3.38, respectively) (Fig. 9A). Regarding GR×SCB interaction, the highest pH values were recorded to UG/UC in 2022 (5.4) and to G-R_1/C-B_1, G-R_1/UC, G-R_2/C-B_1, G-R_2/C-B_2, and UG/C-B_1 in 2023 (ranging 3.61–3.74), with significant similarities ($P<0.05$) among them (Fig. 9A). The lowest pH values were recorded in G-R_1/C-B_1, G-R_2/C-B_1, and UG/C-B_1 in 2022 (3.33, 3.70, and 3.63, respectively), and in G-R_1/C-B_2, G-R_2/UC, UG/C-B_2, and UG/UC in 2023 (3.14, 3.23, 3.20, and 3.19, respectively) (Fig. 9A).

Total soluble solids (TSS; ºBrix) were significantly influenced ($P<0.05$ or 0.001) by all factors except GR in 2022 (Table S1). The strongest effects were attributed to SCB in 2022 (77.87%) and GR in 2023 (68.24%) (Table S1). In 2023, G-R_1 and G-R_2 recorded the highest TSS (6.07 and 6.10, respectively), while UG showed the lowest (5.36) (Fig. 9B). Among SCB treatments, C-B_1 consistently produced the highest TSS (6.67 in 2022; 6.02 in 2023), with a significant similarity ($P<0.05$) to C-B_2 in 2022 (6.41). UC consistently produced the lowest TSS (5.36 in 2022; 5.73 in 2023), significantly similar ($P<0.05$) to C-B_2 in 2023 (5.78) (Fig. 9B). For the GR×SCB, the highest values were consistently recorded in G-R_1/C-B_1 (7.00 in 2022; 6.14 in 2023) and G-R_2/C-B_1 (6.53 in 2022; 6.21 in 2023), with significant similarities among them and to G-R_1/C-B_2 and G-R_2/UC in

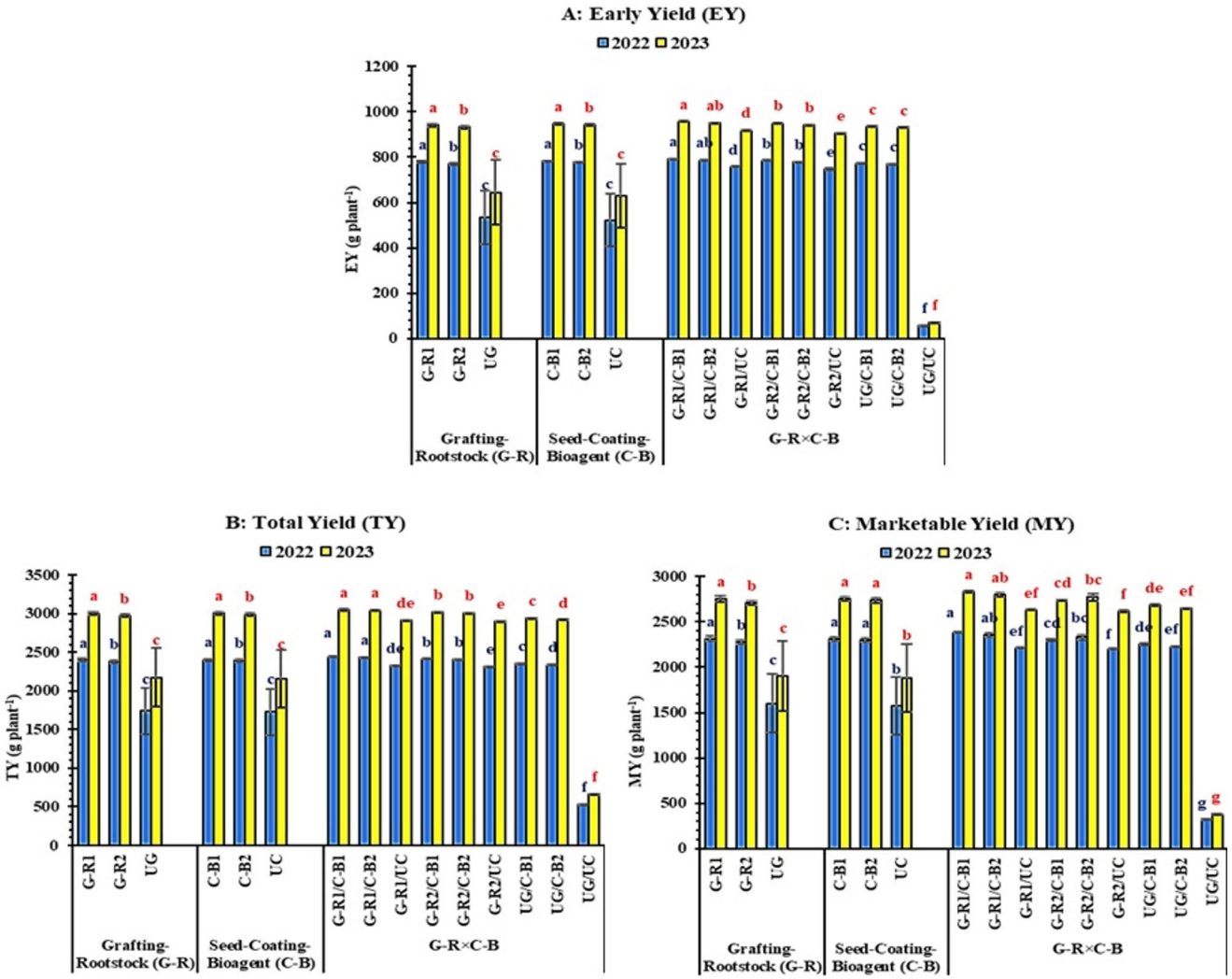

Fig. 8 Effects of grafting and bioagent seed coating on plant yield of tomato 'Apache F_1' under *Meloidogyne incognita* infestation. A: Early, B: total, and C: marketable yield

2023 (6.32 and 6.19, respectively). UG/UC consistently recorded the lowest TSS (5.13 in 2022; 5.23 in 2023), with a significant similarity ($P<0.05$) to UG/C-B_2 in 2023 (5.13) (Fig. 9B).

Fruit dry matter (FDM; mg g^{-1} FW) was highly significantly affected ($P<0.001$) by all factors across both seasons (Table S1). GR was the main contributor (34.8% in 2022; 81.98% in 2023), alongside with SCB in 2022 (36.51%), while GR×SCB had a smaller effect (21.17% in 2022 and 10.62% in 2023) (Table S1). G-R_1 consistently produced the highest FDM (11.72 in 2022; 11.43 in 2023), while UG consistently recorded the lowest (10.08 in 2022; 10.38 in 2023) (Fig. 9C). Among SCB treatments, C-B_1 consistently produced the highest FDM (11.72 in 2022; 11.43 in 2023), while UC consistently recorded the lowest (10.10 and 11.08, respectively), with a significant similarity ($P<0.05$) to C-B_2 in 2023 (11.08) (Fig. 9C). For GR×SCB interaction, the highest FDM values were consistently recorded in G-R1/C-B1 (12.22 in 2022; 11.99 in 2023) and G-R_2/C-B_1 (11.80 in 2022; 11.95 in 2023), with significant similarities ($P<0.05$) to G-R_1/C-B_2 and G-R_1/UC in 2023 (11.91 and 11,96, respectively). UG/UC consistently produced the lowest FDM (8.32 in 2022; 10.41 in 2023), with significant similarities to UG/C-B_1 and UG/C-B_2 in 2023 (10.36 and 10.38, respectively) (Fig. 9C).

Vitamin C (VC; mg Ascorbic Acid 100 g^{-1} FW) was significantly affected ($P<0.05$, 0.01, or 0.001) by all factors, except for SCB in 2023 (Table S1). GR was the main source of variance (35.3% in 2022 and 53.74% in 2023), followed by GR×SCB (28.41% in 2022 and 18.39% in 2023), and SCB (20.79% in 2022; 8.17% in 2023) (Table S1). G-R_1 consistently recorded the highest VC (25.47 in 2022 and 25.97 in 2023), with G-R_2 showing a significantly similar value ($P<0.05$) in 2022 (25.44). UG consistently

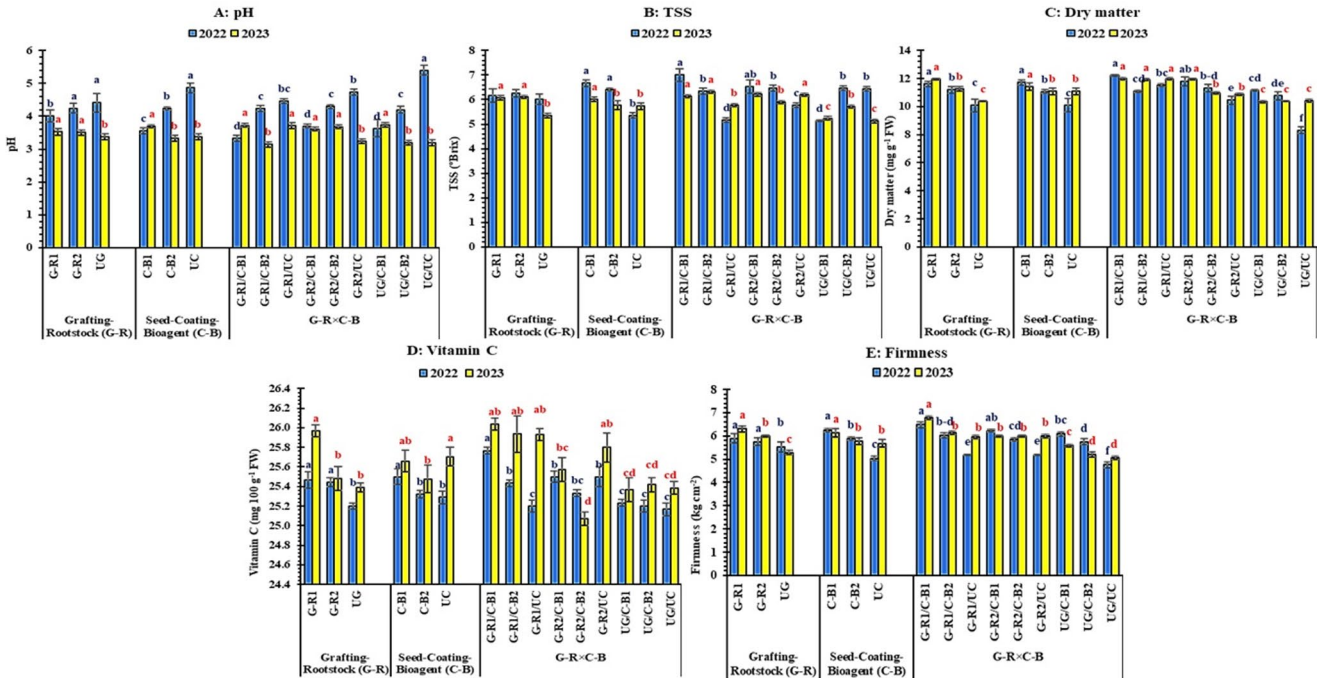

Fig. 9 Effects of grafting and bioagent seed coating on fruit quality of tomato 'Apache F_1' under *Meloidogyne incognita* infestation. A: pH, B: TSS, C: dry matter, D: vitamin C, and E: firmness

recorded the lowest VC (25.20 in 2022; 25.39 in 2023), with G-R_2 showing a significantly similar value ($P<0.05$) in 2023 (25.48) (Fig. 9D). Among SCB treatments, C-B_1 consistently showed the highest VC (25.50 in 2022; 25.66 in 2023), with a significant similarity ($P<0.05$) to UC in 2023 (25.71), whereas C-B_2 consistently recorded the lowest (25.32 in 2022; 25.47 in 2023), with UC showing a significantly similar value ($P<0.05$) in 2022 (25.32) (Fig. 9D). The G-R_1/C-B_1 combination consistently recorded the highest VC (25.77 in 2022; 266.04 in 2023), with significant similarities ($P<0.05$) to G-R1/C-B_2, G-R_1/UC, and G-R_2/UC in 2023 (25.94, 25.93, and 25.80, respectively). The lowest VC values were consistently recorded with G-R_2/C-B_2 (25.33 in 2022; 25.07 in 2023), UG/C-B_1 (25.23 in 2022; 25.37 in 2023), UG/C-B_2 (25.20 in 2022; 25.42 in 2023), and UG/UC (25.17 in 2022; 25.39 in 2023), with significant similarities ($P<0.05$) among them (Fig. 9D).

Fruit firmness (FF; kg cm^{-2}) was significantly affected ($P<0.05$, 0.01, or 0.001) by all factors, with SCB being dominant in 2022 (57.41%) and GR in 2023 (72.40%) (Table S1). G-R_1 consistently produced the highest FF (5.89 in 2022; 6.30 in 2023), with a significant similarity ($P<0.05$) to G-R2 in 2022 (5.75) (Fig. 9E). UG consistently showed the lowest FF (5.53 in 2022; 5.28 in 2023) (Fig. 9E). Among SCB treatments, C-B_1 consistently had the highest FF (6.26 in 2022; 6.13 in 2023), while UC consistently recorded the lowest (5.04 in 2022; 5.67 in 2023), with a significant similarity to C-B_2 in 2023 (5.78) (Fig. 9E). The G-R_1/C-B_1 combination consistently recorded the highest FF (6.48 in 2022; 6.79 in 2023), showing a significant similarity ($P<0.05$) to G-R_2/C-B_1 in 2022 (6.22). The UG/UC combination consistently recorded the lowest FF (4.76 in 2022; 5.05 in 2023), with a significant similarity to UG/C-B_2 in 2023 (5.21) (Fig. 9E).

Photosynthetic pigments and biomass accumulation

High significant effects ($P<0.01$ or 0.001) were observed for GR, SCB, and their interaction on chlorophyll-a (mg g^{-1} FW) in both seasons, with the strongest contributions attributed to GR (22.64% in 2022 and 41.08% in 2023) and SCB (52.24% in 2022 and 25.64% in 2023), while the GR×SCB interaction contributed less (15.84% in 2022 and 16.34% in 2023) (Table S1). Foliar photosynthetic pigments for grafted and ungrafted 'Apache F_1' plants, with or without bioagent-based seed-coating, are presented in Fig. 10. The highest chlor-a contents were consistently recorded in G-R_1 (1.05 in 2022 and 1.31 in 2023), while UG consistently showed the lowest (0.81 in 2022 and 1.07 in 2023) (Fig. 10A). Among SCB treatments, C-B_1 consistently had the highest chlor-a content (1.08 in 2022 and 1.24 in 2023), with a significant similarity ($P<0.05$) to C-B_2 in 2023 (1.25). UC consistently recorded the lowest chlor-a (0.71 in 2022 and 1.07 in 2023; Fig. 10A). The G-R_1/C-B_1 combination consistently recorded the highest chlor-a contents (1.23 in 2022 and 1.36 in 2023), showing a significant similarity

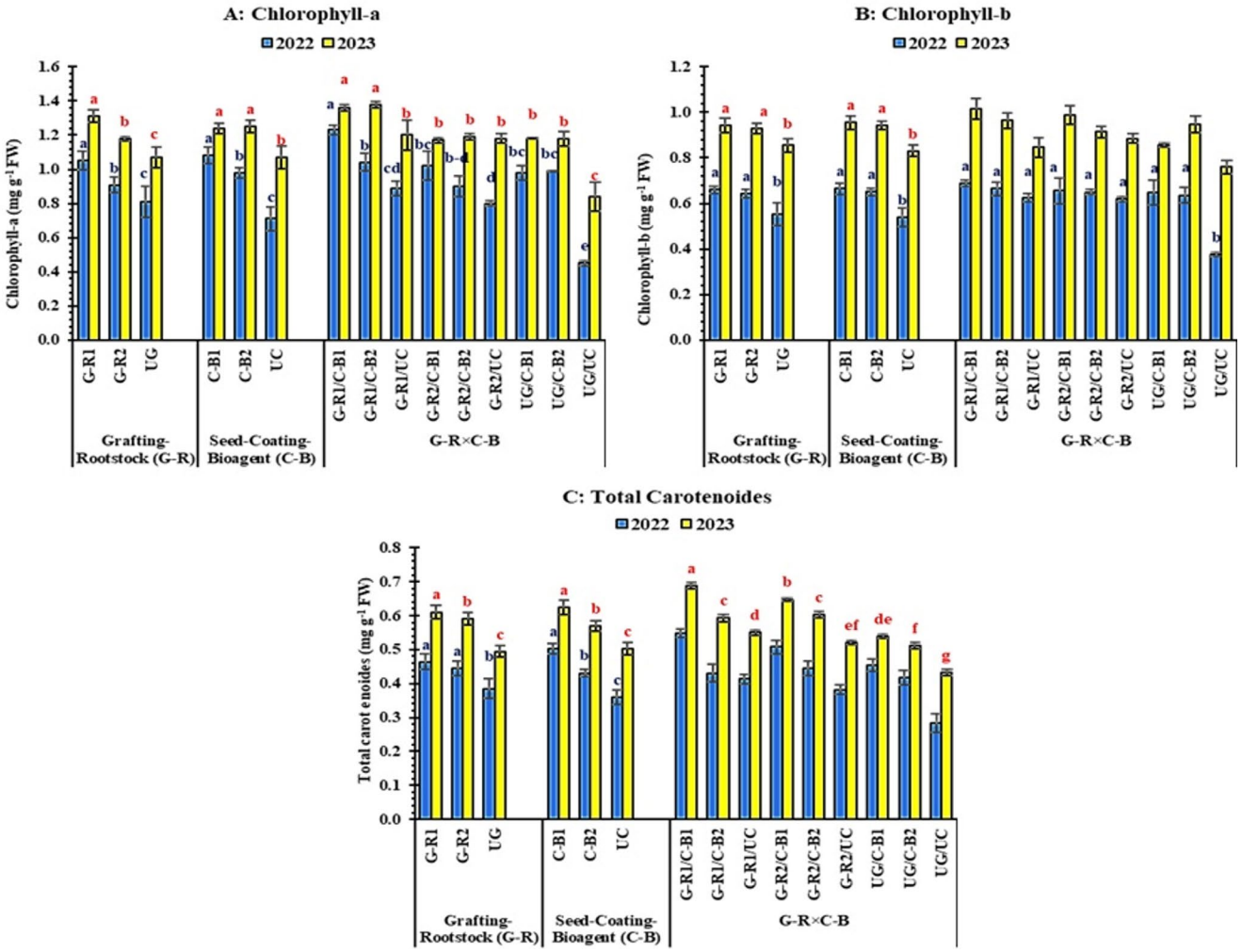

Fig. 10 Effects of grafting and bioagent seed coating on foliar photosynthetic pigment content in tomato 'Apache F_1' under *Meloidogyne incognita* infestation. A: chlorophyll a, B: chlorophyll b, and C: total carotenoids

($P<0.05$) to G-R_1/C-B_2 in 2023 (1.38) (Fig. 10A). The control combination UG/UC consistently recorded the lowest chlor-a contents (0.45 in 2022 and 0.84 in 2023; Fig. 10A).

Chlorophyll-b (chlor-b; mg g^{-1} FW) was significantly affected by GR and SCB ($P<0.05$ or 0.001) in both years, whereas their interaction was highly significant ($P<0.001$) only in 2022. The strongest effects on chlor-b were due to SCB (31.60% in 2022 and 38.32% in 2023), followed by GR (21.56% in 2022 and 19.63% in 2023) and the GR×SCB interaction (26.39% in 2022 and 14.49% in 2023) (Table S1). The highest chlor-b content was consistently recorded in G-R_1 (0.66 in 2022 and 0.94 in 2023) and G-R_2 (0.64 in 2022 and 0.93 in 2023), while UG had the lowest (0.55 in 2022 and 0.85 in 2023; Fig. 10B). The highest chlor-b content in SCB treatments was consistently observed in C-B_1 (0.66 in 2022 and 0.95 in 2023) and C-B_2 (0.65 in 2022 and 0.94 in 2023), with a significant similarity ($P<0.05$) among them, while UC consistently had the lowest (0.54 in 2022 and 0.83 in 2023; Fig. 10B). In 2022, the control combination UG/UC consistently had the lowest chlor-b (0.76), while the other treatments consistently the highest (ranging 0.86–1.02), with significant similarities ($P<0.05$) among them (Fig. 10B).

Total carotenoids (T-Carot; mg g^{-1} FW) were significantly influenced ($P<0.01$ or 0.001) by GR and SCB in both seasons, whereas their interaction was significant ($P<0.05$) only in 2023. The relative contributions of GR (18.71% and 48.60%), SCB (58.71% and 46.52%), and the GR×SCB interaction (7.74% and 2.78%) varied notably between seasons (Table S1). The highest T-Carot content consistently observed in G-R_1 (0.46 in 2022 and 0.61 in 2023), with a significant similarity ($P<0.05$) to G-R_2 in 2022 (0.44), while UC consistently had the lowest (0.39 in 2022 and 0.49 in 2023; Fig. 10D). Among SCB treatments, C-B_1 consistently had the highest t-carot (0.50 in 2022 and 0.62 in 2023), while UC consistently recorded the lowest

(0.36 in 2022 and 0.50 in 2023; Fig. 10D). IN 2023, the G-R_1/C-B_1 combination recorded the highest value (0.69), while UG/UC recorded the lowest (0.43; Fig. 10D).

Across both seasons, GR, SCB, and their interaction had highly significant effects ($P<0.01$ or 0.001) on shoot dry matter content (SDM) and root contents of carbohydrates (RC), proteins (RPr), and polyphenols (RPPh), while root dry matter content (RDM) was significantly influenced by GR only in 2023 (Table S1). The magnitude of these effects varied seasonally: GR exerted the strongest influence on SDM and RDM in 2023 (43.74% and 91.92%, respectively), SCB predominantly determined RPr (45.66% in 2022 and 39.89% in 2023) and RPPh (83.65% in 2022 and 71.07% in 2023) in both seasons, and the GR×SCB interaction had a substantial impact on SDM in 2022 (52.32%) and on RC in both seasons (42.68% and 42.48%, respectively; Table S1). Shoot and root biomass accumulation for grafted and ungrafted 'Apache F_1' plants, with or without bioagent-based seed-coating, are presented in Fig. 11.

The effect of GR on SDM (mg g^{-1}) varied between seasons (Fig. 11A). The highest SDM values were recorded for UG in 2022 (16.25) and for G-R_1 in 2023 (15.13), whereas the lowest were observed in G-R_2 in 2022 (15.37) and UG in 2023 (14.18) (Fig. 11A). The highest SDM values were observed in the SCB treatments C-B_1 (15.94 in 2022 and 14.86 in 2023) and UC (16.02 in 2022 and 14.63 in 2023), with a significant similarity ($P<0.05$) among them, whereas the lowest were consistently recorded in C-B_2 (15.08 in 2022 and 14.36 in 2023) (Fig. 11A). The highest SDM values were observed in combinations UG/UC in 2022 (18.00) and G-R_1/C-B_1 in 2023 (15.72), whereas the lowest were consistently associated with UG/C-B_1 (15.73 in 2022 and 14.12 in 2023) and UG/C-B_2 (15.01 in 2022 and 13.68 in 2023), with significant similarities ($P<0.05$) among them and to G-R_1/C-B_2, G-R_1/UC, and G-R_2/C-B_2 in 2022 (14.95, 15.01, 15.27, and 15.04, respectively) (Fig. 11A).

In 2023, when significant differences in RDM (mg g^{-1}) were detected, G-R_1 exhibited the highest value (15.87), while UG showed the lowest (13.69) (Fig. 11B). The SCB treatments C-B_1 and UC yielded the greatest RDM values (14.88 and 15.12, respectively), with a significant similarity ($P<0.05$) among them, while C-B_2 produced the lowest (14.82) (Fig. 11B). The combinations G-R_1/C-B_1, G-R_1/C-B_2. G-R_1/UC, and G-R_2/UC exhibited the highest RDM values (ranging 15.47–15.95), with significant similarities ($P<0.05$) among them, while the combinations UG/C-B_1 and UG/C-B_2 showed the lowest (13.71 and 13.39, respectively), with a significant similarity ($P<0.05$) among them (Fig. 11B).

The highest RC contents (mg g^{-1}) were recorded with G-R_1 in both seasons (44.05 in 2022 and 48.67 in 2023), with a significant similarity ($P<0.05$) to G-R_2 in 2022 (43.56) (Fig. 11C), whereas the lowest recorded in UG (37.07 and 41.17). The SCB treatment C-B_1 consistently produced the highest RC values (44.22 in 2022 and 48.35 in 2023), with a significant similarity ($P<0.05$) to C-B_2 in 2022 (44.04), while UC consistently showed the lowest (36.42 in 2022 and 41.08 in 2023) (Fig. 11C). The G-R_1/C-B_1 combination

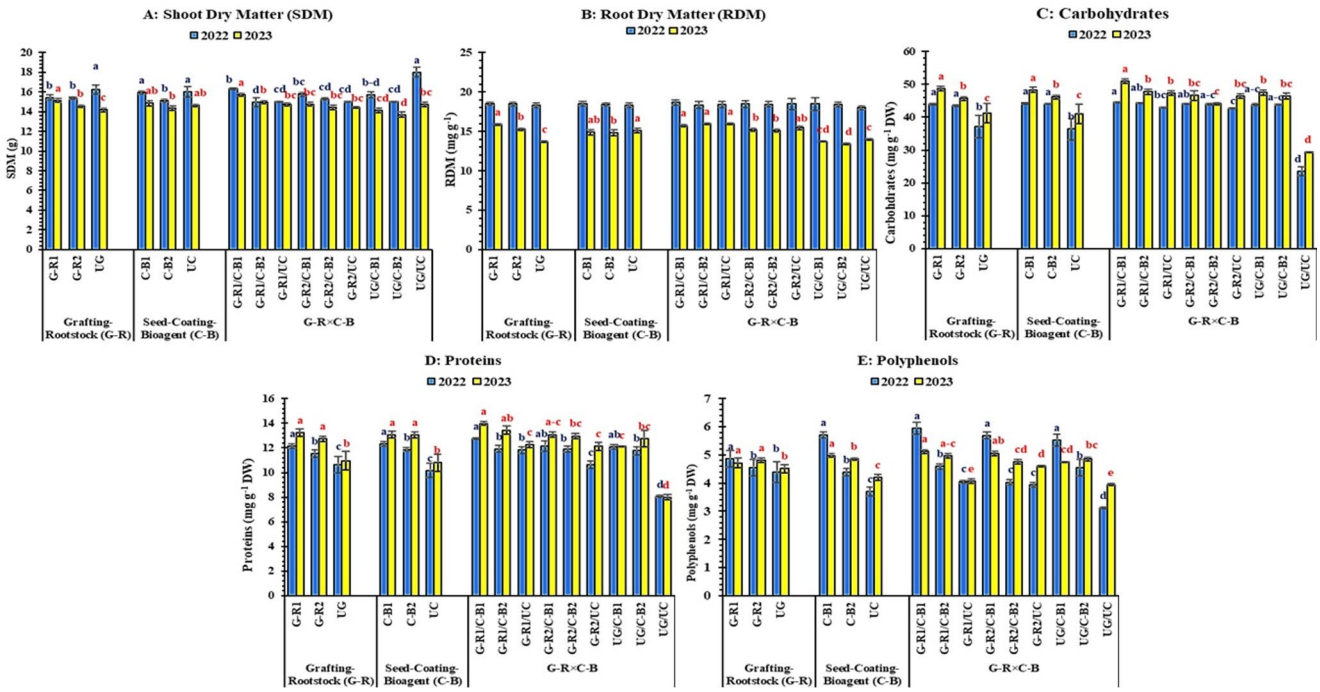

Fig. 11 Effects of grafting and bioagent seed coating on shoot and root biochemical composition of tomato 'Apache F_1' under *Meloidogyne incognita* infestation. A: shoot dry matter, B: root dry matter, and C-E: root content of carbohydrates, proteins, and polyphenols

Table 1 Loadings of the first three principal components for 37 traits of grafted and ungrafted tomato 'Apache F_1' plants with or without bioagent seed coating under *Meloidogyne incognita* infestation

Trait[z]	PC1	PC2	PC3
NG	−0.962	0.268	0.024
NEM	−0.964	0.260	−0.002
SL30	0.946	0.224	0.021
SL60	0.962	0.179	0.137
SD30	0.981	0.012	0.148
SD60	0.987	0.028	0.105
NPL30	0.918	0.220	0.276
NPL60	0.953	0.057	0.287
LA30	0.831	0.538	0.120
LA60	0.829	0.523	0.052
SFW	0.953	−0.281	0.091
SDW	0.992	−0.075	0.029
RFW	0.975	−0.219	0.000
RDW	0.988	−0.119	0.084
DUFFE	−0.982	0.151	−0.048
DUFRFE	−0.978	−0.104	0.005
NFI	0.976	−0.113	−0.164
NFC	0.987	−0.116	−0.065
FSP	0.966	−0.218	0.089
AFW	0.985	−0.159	0.045
EY	0.943	−0.324	0.049
TY	0.949	−0.306	0.055
MY	0.954	−0.292	0.046
pH	0.790	0.143	−0.573
TSS	0.838	0.187	−0.365
FF	0.896	0.336	−0.233
VC	0.574	0.621	0.257
FDM	0.912	0.264	0.143
Chlor-a	0.962	0.037	−0.119
Chlor-b	0.966	−0.041	−0.159
T-Carot	0.897	0.297	−0.243
SDM	−0.411	0.874	−0.219
RDM	0.648	0.440	0.583
RC	0.964	−0.235	0.027
RPr	0.982	−0.117	−0.076
RPPh	0.790	0.143	−0.573

[z]Trait was NG: number of galls; NEM: number of egg masses; SL30 and SL60: stem length at 30 and 60 days after transplanting (DAT); SD30 and SD60: stem diameter at 30 and 60 DAT; NPL30 and NPL60: number of plant leaves at 30 and 60 DAT; LA30 and LA60: leaf area at 30 and 60 DAT; SFW and SDW: shoot fresh and dry weights; RFW and RDW: root fresh and dry weights; DFFE: days to first flower emission; DFRFE: days to first ripened fruit emission; NFI: number of flowers per inflorescence; NFC: number of fruits per cluster; FSP: fruit set percentage; AFW: average fruit weight; EY, TY, and MY: early, total, and marketable yield, respectively; pH: fruit juice pH; TSS: total soluble solids in fruit; FF: fruit firmness; VC: fruit vitamin C content; and DM: fruit dry matter content; Chlor-a and Chlor-b: leaf content of chlorophyll a and b, respectively; Chlor-a/b: ratio of chlorophyll a to b; T-Carot: leaf total carotenoids content; SDM: shoot dry matter; RDM: root dry matter; RC, RPr, and RPPh: root content of carbohydrates, protein, and polyphenols, respectively

Bold eigenvector values of PCs indicate a significant correlation between the variable and principal component

consistently recorded the greatest RC (44.71 in 2022 and 50.92 in 2023), with significant similarities ($P<0.05$) to G-R_1/C-B_2, G-R_2/C-B_2, UG/C-B_1, and UG/C-B_2 in 2022 (ranging 43.84–44.37). The lowest RC value was consistently recorded in UG/UC combination (23.53 in 2022 and 29.48 in 2023) (Fig. 11C).

The highest RPr contents (mg g^{-1}) were consistently recorded with G-R_1 (12.17 in 2022 and 13.23 in 2023), with a significant similarity ($P<0.05$) to G-R_2 in 2022 (12.73), while UC consistently showed the lowest (10.63 in 2022 and 10.96 in 2023) (Fig. 11D). The SCB treatment C-B_1 consistently produced the highest RPr (12.31 in 2022 and 13.06 in 2023), with a significant similarity ($P<0.05$) to C-B_2 in 2023 (13.06), while UC consistently showed the lowest (10.17 in 2022 and 10.80 in 2023) (Fig. 11D). The G-R_2/C-B_1 combination recorded the highest RPr (12.13 in 2022 and 13.08 in 2023), with significant similarities ($P<0.05$) to UG/C-B_1 in 2022 (12.06) and G-R_1/C-B_2 in 2023 (13.44) (Fig. 11D). The lowest RPr values were consistently observed with UG/UC (8.05 in 2022 and 8.00 in 2023) (Fig. 11D).

The highest RPPh contents (mg g^{-1}) was consistently recorded in G-R_1 (4.86 in 2022; 4.72 in 2023), with G-R_2 showing a significantly similar ($P<0.05$) value in 2023 (4.81) (Fig. 11E). The lowest RPPh was consistently observed with UG (4.39 in 2022; 4.52 in 2023). The SCB treatment C-B_1 consistently produced the highest RPPh (5.72 in 2022; 4.98 in 2022), whereas UC consistently recorded the lowest (3.70 in 2022; 4.21 in 2023) (Fig. 11E). The greatest RPPh values were consistently recorded in the combinations G-R_1/C-B_1 (5.94 in 2022; 5.12 in 2023) and G-R_2/C-B_1 (5.69 in 2022; 5.06 in 2023), with significant similarities ($P<0.05$) among them and to UG/C-B_1 in 2022 (5.52) and G-R_1/C-B_2 in 20,233 (4.96). The UG/UC combination exhibited the lowest RPPh values (3.12 in 2022 and 3.95 in 2023), with a significant similarity to G-R_1/UC in 2023 (4.07) (Fig. 11E).

Principal Component Analysis

Eight principal components (PCs) were identified, with eigenvalues ranging from 31.01 to 0.07 (Fig. S2). The first three PCs had eigenvalues > 1 and accounted for 97.06% of the total variance (Fig. S2). Trait loadings are presented in Table 1. All measured parameters significantly contributed to PC1 and PC2. PC1 explained 83.82% of the total variance (eigenvalue = 31.01; Fig. S2), with negative loadings for NG, NEM, DFFE, and DFRFE (ranging from −0.962 to −0.982) and positive loadings for the remaining traits (ranging from 0.648 to 0.988), except for VC and SDM (Table 1). PC2 accounted for 8.55% of the variance (eigenvalue = 3.16; Fig. S2), with positive loadings for VC (0.621)

and SDM (0.874; Table 1). PC3 contributed 1.14% of the total variance (eigenvalue = 1.74; Fig. S2).

Figure 12 shows the PCA-biplot of the first two PCs, illustrating the distribution of the combination treatments and the estimated traits. The vectors for NG, NEM, SDM, and DFFE were grouped in one quadrant, while DFRFE was positioned in a separate quadrant; however, all were oriented in similar directions with angles below 90° (Fig. 12). The remaining trait vectors were located in two opposite quadrants, positioned close together with similar orientations (Fig. 12).

Significant correlations among the estimated traits were identified using Pearson's correlation coefficients, as shown in Table 2. NG and NEM showed a highly significant ($P < 0.001$) positive correlation with each other ($r = 0.999$). Both traits also exhibited highly significant ($P < 0.001$) positive correlations with DFFE (0.982 and 0.985, respectively) and DFRFE (0.915 and 0.912, respectively), while NEM alone showed a significant ($P < 0.05$) positive correlation with SDM (0.585). In contrast, NG and NEM showed highly significant ($P < 0.01$ or 0.001) negative correlations with vegetative growth traits (SL30: 0.854 and −0852, SL60: 00.882 and 0.893, SD30: 0.939 and 0.944, SD60: 0.941 and 0.946, NPL30: 0.810 and 0.819, NPL: 0.810 and 0.819, NPL60: 0.891 and 0.900, LA30: 0.682 and 0.691, LA60: 0.676 and 0.677, SFW: 0.991 and 0.991, SDW: 0.975 and 0.973, RFW: 0.998 and 0.997, and RDW: 0.981 and 0.985), yield (EY: 0.993 and 0.992, TY: 0.994 and 0.994,

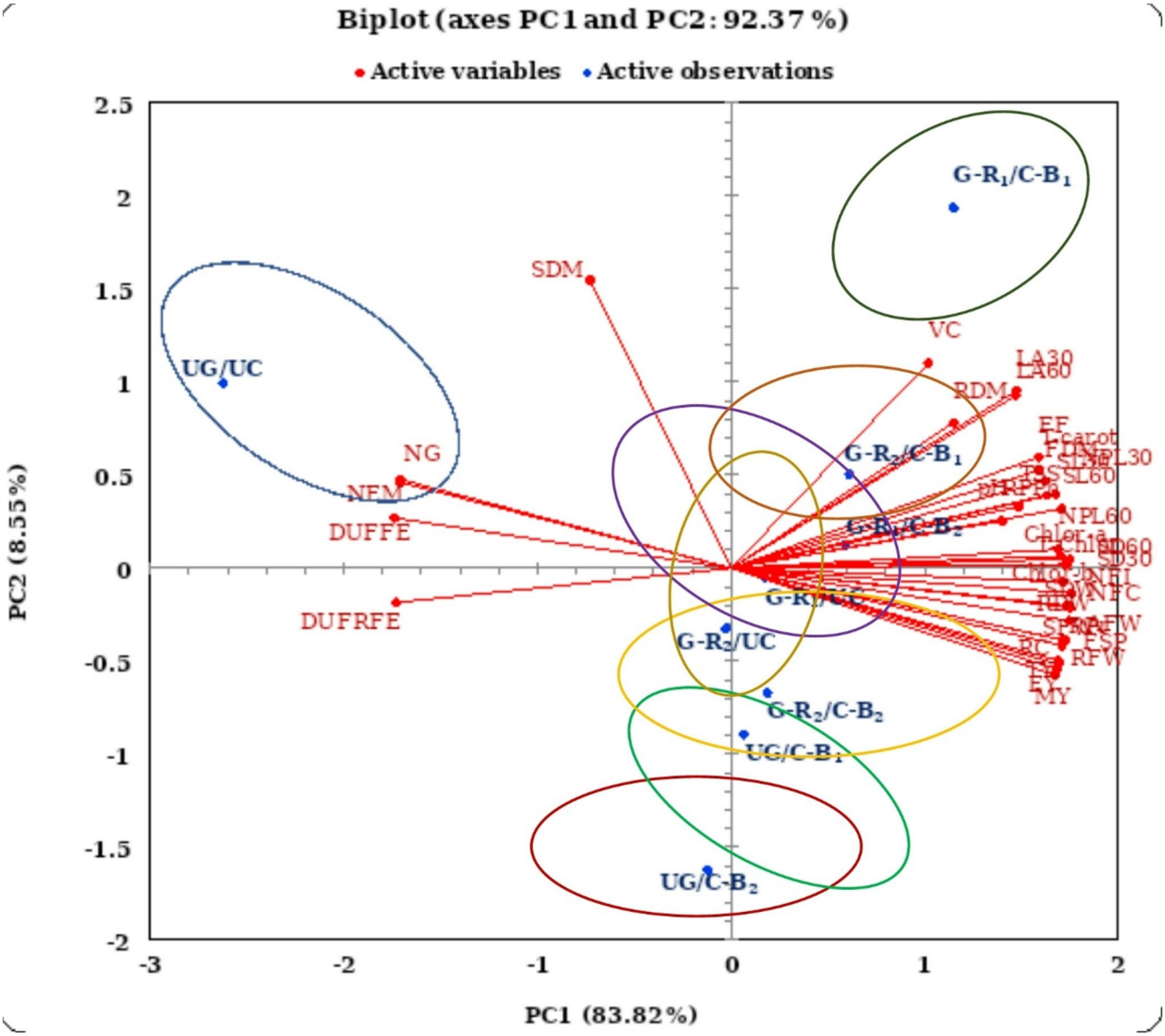

Fig. 12 Biplot between the first two principal components for 37 traits of grafted and ungrafted tomato 'Apache F_1' plants with or without bioagent seed coating under *Meloidogyne incognita* infestation

Table 2 Pearson's correlation coefficients between estimated traits of grafted and ungrafted 'Apache F_1' tomato plants, with or without seed-coating using bioagents, under *Meloidogyne incognita* infestation

Trait[z]	NG	NEM	SL30	SL60	SD30	SD60	NPL30	NPL60	LA30	LA60	SFW	SDW	RFW	RDW	DFFE	DFRFE	NFI	NFC
NG	1																	
NEM	0.999***	1																
SL30	-0.854***	-0.852***	1															
SL60	-0.882***	-0.893***	0.926***	1														
SD30	-0.939***	-0.944***	0.941***	0.975***	1													
SD60	-0.941***	-0.946***	0.944***	0.981***	0.997***	1												
NPL30	-0.810***	-0.819***	0.923***	0.951***	0.930***	0.930***	1											
NPL60	-0.891***	-0.900***	0.924***	0.968***	0.978***	0.970***	0.974***	1										
LA30	-0.682**	-0.691**	0.923***	0.926***	0.864***	0.873***	0.927***	0.879***	1									
LA60	-0.676**	-0.677**	0.928***	0.894***	0.850***	0.859***	0.910***	0.852***	0.979***	1								
SFW	-0.991***	-0.991***	0.862***	0.882***	0.949***	0.946***	0.834***	0.917***	0.687**	0.678**	1							
SDW	-0.975***	-0.973***	0.946***	0.939***	0.982***	0.982***	0.898***	0.949***	0.813***	0.814***	0.976***	1						
RFW	-0.998***	-0.997***	0.881***	0.905***	0.958***	0.960***	0.841***	0.914***	0.722**	0.718**	0.992***	0.986***	1					
RDW	-0.981***	-0.985***	0.916***	0.948***	0.985***	0.984***	0.897***	0.959***	0.795***	0.778***	0.984***	0.993***	0.990***	1				
DFFE	0.982***	0.985***	-0.903***	-0.932***	-0.967***	-0.973***	-0.888***	-0.941***	-0.773***	-0.755***	-0.983***	-0.985***	-0.990***	-0.992***	1			
DFRFE	0.915***	0.912***	-0.982***	-0.941***	-0.965***	-0.966***	-0.926***	-0.945***	-0.884***	-0.890***	-0.912***	-0.977***	-0.936***	-0.957***	0.948***	1		
NFI	-0.973***	-0.970***	0.879***	0.902***	0.926***	0.940***	0.827***	0.872***	0.747***	0.755***	0.942***	0.965***	0.976*****	0.960***	-0.967***	-0.936***	1	
NFC	-0.983***	-0.983***	0.897***	0.925***	0.951***	0.959***	0.867***	0.913***	0.770***	0.771***	0.966***	0.982***	0.987***	0.981***	-0.983***	-0.949***	0.994***	1
FSP	-0.987***	-0.989***	0.879***	0.904***	0.955***	0.953***	0.870***	0.934***	0.727**	0.719**	0.994***	0.981***	0.990***	0.988***	-0.985***	-0.927***	0.954***	0.979***
AFW	-0.990***	-0.993***	0.895***	0.937***	0.975***	0.977***	0.871***	0.939***	0.766***	0.750***	0.987***	0.989***	0.996***	0.998***	-0.992***	-0.943***	0.970***	0.986***
EY	-0.993***	-0.992***	0.840***	0.858***	0.930***	0.928***	0.806***	0.891***	0.650**	0.645**	0.998***	0.966***	0.991***	0.975***	-0.978***	-0.898***	0.947***	0.965***
TY	-0.994***	-0.994***	0.849***	0.868***	0.937***	0.935***	0.816***	0.900***	0.665**	0.657**	0.999***	0.971***	0.993***	0.979***	-0.981***	-0.905***	0.948***	0.968***
MY	-0.996***	-0.996***	0.854***	0.875***	0.941***	0.940***	0.818***	0.902***	0.674**	0.667**	0.999***	0.974***	0.995***	0.982***	-0.982***	-0.909***	0.953***	0.971***
pH	-0.454	-0.446	0.463	0.416	0.409	0.431	0.384	0.367	0.392	0.418	0.415	0.463	0.455	0.435	-0.456	-0.48	0.521	0.496*
TSS	-0.809***	-0.806***	0.850***	0.805***	0.791***	0.805***	0.695**	0.727***	0.764***	0.739**	0.759***	0.837***	0.811***	0.816***	-0.805***	-0.860***	0.868***	0.854***
FF	-0.813***	-0.810***	0.927***	0.904***	0.878***	0.889***	0.826***	0.828***	0.900***	0.902***	0.773***	0.884***	0.832***	0.858***	-0.837***	-0.932***	0.891***	0.881***
VC	-0.401	-0.418	0.664**	0.715**	0.594*	0.606*	0.808***	0.684***	0.843***	0.825***	0.418	0.539*	0.439	0.527*	-0.509	-0.611*	0.489	0.533
FDM	-0.813***	-0.819***	0.933***	0.963***	0.942***	0.949***	0.950***	0.942***	0.939***	0.919***	0.819***	0.898***	0.847***	0.896***	-0.892***	-0.939***	0.847***	0.862***
Chlor-a	-0.924***	-0.926***	0.865***	0.939***	0.928***	0.941***	0.853***	0.881***	0.811***	0.817***	0.889***	0.935***	0.933***	0.935***	-0.926***	-0.916***	0.972***	0.969***
Chlor-b	-0.952***	-0.955***	0.883***	0.921***	0.926***	0.945***	0.813***	0.862***	0.781***	0.764***	0.924***	0.951***	0.956***	0.951***	-0.956***	-0.915***	0.976***	0.972***
T-Carot	-0.815***	-0.810***	0.940***	0.892***	0.881***	0.899***	0.815***	0.817***	0.889***	0.896***	0.782***	0.888***	0.839***	0.857***	-0.854***	-0.938***	0.889***	0.871***
SDM	0.58	0.585*	-0.146	-0.242	-0.37	-0.357	-0.192	-0.348	0.109	0.143	-0.611*	-0.423	-0.543*	-0.48	0.505	0.244	-0.42	-0.449
RDM	-0.511	-0.534*	0.737***	0.793***	0.742**	0.722**	0.852***	0.831***	0.854***	0.776***	0.571*	0.642**	0.552*	0.661**	-0.617*	-0.691**	0.486	0.557
RC	-0.990***	-0.988***	0.870***	0.891***	0.945***	0.947***	0.853***	0.913***	0.708**	0.717**	0.989***	0.979***	0.992***	0.980***	-0.983***	-0.925***	0.970***	0.986***
RPr	-0.980***	-0.979***	0.889***	0.930***	0.961***	0.970***	0.838***	0.901***	0.767***	0.767***	0.960***	0.977***	0.986***	0.979***	-0.976***	-0.940***	0.986***	0.986***
RPPh	-0.745***	-0.730**	0.770***	0.694**	0.681**	0.716**	0.622*	0.602*	0.660**	0.702**	0.672**	0.762***	0.748***	0.717**	-0.746***	-0.803***	0.863***	0.814***

Trait[z]	NFC	FSP	AFW	EY	TY	MY	pH	TSS	FF	VC	FDM	Chlor-a	Chlor-b	T-Carot	SDM	RDM	RC	RPr	RPPh
NFC	1																		
FSP	0.979***	1																	
AFW	0.986***	0.989***	1																
EY	0.965***	0.990***	0.981***	1															
TY	0.968***	0.992***	0.985***	1.000***	1														
MY	0.971***	0.993***	0.988***	0.999***	1.000***	1													
pH	0.496*	0.433	0.443	0.425	0.425	0.429	1												
TSS	0.854***	0.781***	0.819***	0.754***	0.765***	0.776***	0.520*	1											
FF	0.881***	0.801***	0.850***	0.757***	0.769***	0.781***	0.508	0.943***	1										
VC	0.533	0.502*	0.494	0.379	0.395	0.4	0.275	0.49	0.634*	1									
FDM	0.862***	0.833***	0.876***	0.793***	0.803***	0.807***	0.407	0.740**	0.881***	0.688**	1								
Chlor-a	0.969***	0.914***	0.943***	0.884***	0.889***	0.898***	0.495	0.850***	0.917***	0.603*	0.869***	1							
Chlor-b	0.972***	0.933***	0.962***	0.922***	0.927***	0.933***	0.506	0.901***	0.902***	0.511	0.850***	0.959***	1						
T-Carot	0.871***	0.794***	0.850***	0.769***	0.778***	0.787***	0.516*	0.906***	0.974***	0.564*	0.910***	0.888***	0.905***	1					
SDM	-0.449	-0.564	-0.51	-0.638*	-0.626**	-0.613*	-0.062	-0.12	-0.007	0.238	-0.131	-0.3	-0.389	-0.032	1				
RDM	0.557	0.604*	0.616*	0.516*	0.535*	0.539*	0.138	0.484	0.619*	0.787***	0.794***	0.558*	0.531	0.582*	-0.003	1			
RC	0.986***	0.994***	0.985***	0.989***	0.990***	0.990***	0.456	0.773***	0.803***	0.477	0.828***	0.928***	0.937***	0.804***	-0.557*	0.540*	1		
RPr	0.986***	0.960***	0.987***	0.958***	0.960***	0.965***	0.478	0.841***	0.884***	0.469	0.877***	0.968***	0.978***	0.893***	-0.443	0.544*	0.970***	1	
RPPh	0.814***	0.697***	0.730**	0.688**	0.689**	0.696**	0.595*	0.881***	0.871***	0.424	0.690**	0.825***	0.837***	0.884***	-0.055	0.228	0.737**	0.798***	1

[z] Trait was NG: number of galls; NEM: number of egg masses; SL30 and SL60: stem length at 30 and 60 days after transplanting (DAT); SD30 and SD60: stem diameter at 30 and 60 DAT; NPL30 and NPL60: number of plant leaves at 30 and 60 DAT; LA30 and LA60: leaf area at 30 and 60 DAT; SFW and SDW: shoot fresh and dry weights; RFW and RDW: root fresh and dry weights; DFFE: days to first flower emission; DFRFE: days to first ripened fruit emission; NFI: number of flowers per inflorescence; NFC: number of fruits per cluster; FSP: fruit set percentage; AFW: average fruit weight; EY, TY, and MY: early, total, and marketable yield, respectively; pH: fruit juice pH; TSS: total soluble solids in fruit; FF: fruit firmness; VC: fruit vitamin C content; and DM: fruit dry matter content; Chlor-a and Chlor-b: leaf content of chlorophyll a and b, respectively; Chlor-a/b: ratio of chlorophyll a to b; T-Carot: leaf total carotenoids content; SDM: shoot dry matter; RDM: root dry matter; RC, RPr, and RPPh: root content of carbohydrates, protein, and polyphenols, respectively.
*, **, *** Significant at 0.05, 0.01, and 0.001 probability levels, respectively.
Red, white, and blue color gradients indicate the lowest (-1), moderate (0), and highest (+1) correlation coefficients, respectively.

and MY: 0.996 and 0.996), yield components (NFI: 0.973 and 0.970, NFC: 0.983 and 0.983, FSP: 0.987 and 0.989, and AFW: 0.990 and 0.993), fruit quality (TSS: 0.908 and 0.806, FF: 0.813 and 0.810, and FDM: 0.813 and 0.819), leaf content of photosynthetic pigments (Chlor-a: 0.924 and 0.926, Chlor-b: 0.952 and −0.955, and T-Carot: 0.815 and 0.810), and root content of carbohydrates (0.990 and 0.988), proteins (0.980 and 0.979), and polyphenols (0.745 and 0.730). Additionally, NEM alone was negatively correlated with RDM (−0.534) (Table 2).

UG/UC clustered in the upper-left quadrant near NG, NEM, DUFFE, DUFRFE, and SDM vectors (Fig. 12). In contrast, G-R_1/C-B_1, G-R_1/C-B_2, and G-R_2/C-B_1 occupied the upper right quadrant, aligning with vectors representing vegetative growth (SL30, SL60, SD30, SD60, NPL30, NPL60, LA30, and LA60), photosynthetic pigments (Chlor-a and T-Carot), root biochemical traits (RDM and PPh), and fruit quality (FF, FDM, TSS, pH, and VC). G-R_1/UC, G-R_2/C-B_2, G-R_2/UC, and UG/C-B_1 clustered in the lower-right quadrant close to the vectors of biomass accumulation (SFW, SDW, RFW, RDW), Chlor-b, Carb, NFI, yield components (NFC, FSP, AFW), yield (EY, TY, and MY) (Fig. 13). UG/C-B_2 was positioned in the lower-left quadrant, closely linked to DUFRFE (Fig. 12).

Discussion

Root-knot nematodes (RKNs) are among the most destructive plant-parasitic nematodes, causing substantial yield losses in numerous crops worldwide, with global economic impacts exceeding US$150 billion annually and accounting for about 12.3% of total crop losses (Lopes-Caitar et al. 2019; Singh et al. 2015). RKN infection induces gall formation in tomato roots, disrupting water and nutrient uptake and creating specialized feeding sites for adult female nematodes. This often results in leaf chlorosis, wilting, stunted growth, floral abortion, reduced fruit yield and quality, and, in severe cases, plant death (Banora 2023). Vegetative

growth and productivity thus serve as key indicators of plant resistance or tolerance to RKNs.

Biological control has emerged as a pivotal component of INM. In Egypt, several soil-isolated microbial agents from genera such as *Bacillus*, *Paenibacillus*, *Pseudomonas*, *Streptomyces*, as well as isolates including *Sporosarcina psychrophile* Sd4-11 and *Streptomyces scabiei* Wb1n-4, have demonstrated significant efficacy in suppressing RKN populations while simultaneously enhancing tomato growth (Adam et al. 2014; Mahmoud et al. 2025a). Furthermore, grafting onto resistant rootstocks, particularly interspecific hybrids like 'Estamino' and 'Fortamino' (*Mi*−1/*mi*−1), provides effective protection against *M. incognita* (Bajek and Rudoph 2023; Mahmoud et al. 2025b). These rootstocks also confer resistance to major soilborne pathogens, including *Verticillium dahliae*, *Fusarium oxysporum* f. sp. *lycopersici*, *F. oxysporum* f. sp. *radicis-lycopersici*, and *Ralstonia solanacearum* (https://www.enzazaden.com/).

Given the limited research on the integrated application of grafting and biological control, this study evaluated the efficacy of *S. psychrophile* Sd4-11 and *S. scabiei* Wb1n-4 against RKN in tomato plants grafted onto resistant interspecific hybrids 'Estamino' and 'Fortamino' versus ungrafted controls. The seed-coatings bioagents (SCB) technique was employed as a high-precision, low-input delivery system to establish a protective biological envelope at the onset of germination. At the seed–soil interface, this envelope promotes early rhizosphere colonization and the formation of a competitive barrier that suppresses RKN infection during the most vulnerable stages of plant growth (Adam et al. 2014). This protective efficacy is further reinforced by the induction of systemic resistance (ISR) and the enhancement of germination and seedling vigor (Mahmoud et al. 2025a).

The study was conducted during the 2022 and 2023 fall seasons in a naturally RKN-infested greenhouse with a documented history of monoculture known to sustain high resident populations of *Meloidogyne* spp. To ensure the empirical validity of the resistance trials, the nematode population was morphologically characterized and quantified prior to transplanting to establish a standardized baseline of initial inoculum pressure (*Pi*). Morphological validation based on perineal pattern analysis identified the nematode population as *M. incognita* (Kofoid and White) Chitwood, consistent with its status as the predominant RKN species in Egyptian agriculture (Abd-Elgawad, 2014; El-Sappah et al., 2019). The consistent presence of a high, squarish dorsal arch and wavy cuticular striae, together with the absence of lateral incisures, provided robust taxonomic discrimination from the morphologically similar *M. javanica* (Taylor and Netscher, 1974). The P_i values recorded across both seasons were exceptionally high (1325–1503 J_2 100 g^{-1} soil). These values far exceed the established damage threshold for tomato, which is typically cited between 1 and 10 J_2 100 g^{-1} soil (Greco and di Vito 2009). Such substantial inoculum pressure enabled a rigorous assessment of host plant responses, providing a clear differentiation between the tested resistant and susceptible genotypes under extreme field-simulated conditions.

A factorial experiment conducted across both seasons evaluated the individual and combined effects of grafting-mediated genetic resistance and seed-coating bioagents on nematode suppression, vegetative growth, and productivity. Data were initially subjected to a pooled ANOVA to assess the significance of year (Y) effects and their interactions with other experimental factors **(**Wickens and Keppek 2004**).** The pooled ANOVA revealed significant effects of Y, GR, and SCB on most evaluated traits, with a significant GR×SCB interaction, indicating strong synergistic effects between these factors. The results also demonstrated pronounced sensitivity to seasonal variation, as Y, its two-way interactions (Y × GR and Y × SCB), and the three-way interaction (Y × GR × SCB) significantly influenced most variables. Consequently, separate analyses were conducted for each season to ensure accurate mean comparisons (Wickens and Keppek 2004). Calculation of sum-of-squares percentages (SS%) further quantified the relative contributions of GR, SCB, and their interactions to the observed trait variation.

Seed coating with bioagents achieved the strongest suppression of RKN infection in the susceptible tomato 'Apache F_1' (Table S1), significantly reducing root galling and egg-mass formation relative to UC controls (Fig. 1) and outperforming grafting alone (Table S1). These findings contrast with previous studies reporting that nematode suppression was primarily attributed to grafting and its interaction with bioagents, while bioagents alone showed no significant effect (Cukrov et al. 2021, Pontes et al. 2024). In this study, both bioagents exhibited comparable suppressive effects under SCB (Fig. 1), likely mediated through direct microbial antagonism and the priming of jasmonic acid- and salicylic acid-dependent defense pathways. This early-stage priming at the seedling phase enhances lignification and the accumulation of inhibitory secondary metabolites, thereby restricting *M. incognita* penetration and development (Adam et al. 2014; Mahmoud et al. 2025a; Sharma et al. 2019, 2025). Furthermore, SCB-mediated suppression proved more resilient than *Mi*-1-mediated rootstock resistance under the high-temperature stress (> 30 ℃) encountered during the first and last two months of trail (Fig. S1). Although GR significantly reduced nematode infection (Table S1), elevated temperatures likely attenuated this temperature-sensitive resistance (Williamson and Roberts 2009; Bajek and Rudoph 2023). Interestingly, despite all rootstocks carrying the *Mi*-1/*mi*−1 genotype, suppressive efficacy varied, with G-R_1 showing

superior performance (Fig. 1). This suggests that additional genetic or physiological factors modulate the phenotypic expression of *Mi*−1-mediated resistance (Bajek and Rudolph 2023; Kokalis-Burelle and Rosskopf 2011; Mahmoud et al. 2025b; Owusu et al. 2016). The combined application of GR and SCB produced synergistic effects (Table S1). Root galling remained below 100 in treated plants across booth seasons, compared with 302.19 and 358.97 in the UG/UC control (Fig. 1A). Similarly, NEM were also below 100 in most treated combinations across both seasons, which contrasted sharply with the high values observed in the UG/UC control (310.87 and 404.88; Fig. 1B). According to the classification indices of Taylor and Sasser (1978), the UG/UC control reached peak infection (GI and EMI = 5), while SCB and GR mitigated RKN infection severity to an index of 4. This indicates that these approaches function as suppressive rather than immunity-conferring strategies. The persistence of infection at 180 DAT reflects the accumulation of multiple *M. incognita* generations and sustained thermal stress near the nematode's developmental optimum. Consequently, the final infection levels represent the biological limits of host defense under prolonged exposure and adverse environmental conditions rather than treatment failure, underscoring the importance of incorporating temporal and thermal dynamics into evaluations of INM strategies.

Grafting exerted the strongest overall influence on vegetative growth traits, including stem length, stem diameter, leaf number, and leaf area, while biomass accumulation reflected complementary contributions from both grafting and seed coating (Table S1). Consistent with previous studies showing that grafting and its interaction with bioagents strongly affect plant development (Cukrov et al. 2021; Pontes et al. 2024), grafting the susceptible cultivar 'Apache F_1' onto resistant rootstock markedly enhanced vegetative growth under RKN infestation (Figs. 2 and 3). These improvements likely stem from the ability of deep-rooted, RKN-resistant interspecific hybrids to restrict nematode penetration and reproduction, thereby maintaining efficient water and nutrient uptake (Bajek and Rudoph 2023; Djidonou et al. 2017; Mahmoud et al. 2025b). Comparable benefits have been reported for other interspecific rootstocks such as 'Multifort,' 'Arnold,' and 'Maxifort,' although some combinations, such as those involving 'Aloha,' may reduce biomass (Kokalis-Burelle and Rosskopf 2011). SCB also significantly promoted vegetative growth, with C-B_1, and to a slightly lesser extent C-B_2, producing the greatest stem length (Fig. 2A-B), stem diameter (Fig. 2C-D), leaf number (Fig. 3A-B), leaf area (Fig. 4C-D), and shoot and root biomass (Fig. 5) compared with the UC control. Notably, the combined application of GR and SCB, particularly G-R_1/C-B_1, generated the highest values across all vegetative parameters, whereas the UG/UC combination consistently produced the lowest (Figs. 2, 3, 4 and 5), demonstrating the strong synergistic advantage of integrating resistant rootstocks with bioagent seed coatings to maximize vegetative performance under RKN-infested greenhouse conditions.

Morphodynamics describes the quantitative integration of plant morphological development and growth kinetics, using changes in traits such as stem elongation, stem thickness, and leaf expansion to evaluate how external treatments or biotic stressors influence plant ontogeny (Hunt 1990). Growth rate metrics (SER, STR, LFR, and LER) provide a comprehensive assessment of canopy architecture and resource partitioning (Arshad et al.2024; Mahmoud 2020; Mahmoud et al. 2025b). In this study, growth rates were governed by complex, trait-specific interactions (Table S1). SER responded most markedly to GR, particularly in 2023 (Table S1), with G-R_1 significantly outperformed the UG control and exhibited further enhancement when combined with SCBs such as C-B_2 (Fig. 4A). STR was primarily influenced by the GR × SCB interaction, while LFR and LER exhibited significant year-dependent variation (Table S1). Interestingly, UG and UC plants maintained robust STR, LFR, and LER (Fig. 4) despite demonstrating significantly inferior overall growth and yields (Figs. 2, 3, 5, 7 and 8). This physiological disparity suggests an inefficient stress-induced morphogenic response (SIMR), a compensatory mechanism where plants reallocate carbon toward vegetative expansion to mitigate root dysfunction caused by *Meloidogyne* spp. Infestation (Potters et al. 2007; Zandalinas et al. 2018). Although this strategy increases the photosynthetic surface area, the nematode-compromised root systems in UG/UC treatments fail to support the heightened transportational and nutritional demands required for fruit loading (Kyriacou et al. 2017). Consequently, photoassimilates remain sequestered within vegetative structures rather than being translocated to reproductive sinks (Melakeberhan 2004). This physiological bottleneck was effectively bypassed by the grafted and bio-coated treatments, which successfully synchronized vigorous vegetative growth with high reproductive output (Abd-Elgawad 2020; Grieneisen et al. 2018).

Reproductive development (DFFE and DFRFE) and yield performance (NF/I, NF/C, FSP, AFW, EY, TY, and MY) exhibited clear and complementary responses to GR and SCB, with each factor exerting trait-specific effects (Table S1). SCB had the greatest influence on DFFE, whereas GR primarily determined the variation in DFRFE (Table S1). The season-dependent G-R × SCB interaction suggests that microbial coatings may influence hormone-regulated reproductive pathways. Treatments that effectively reduced galling and egg-mass formation (Fig. 1) also accelerated flowering and fruit ripening (Fig. 6), linking improved reproductive timing to the alleviation of RKN-induced

physiological constraints. Individually, G-R_1 grafting and C-B_1 seed coating promoted earlier flowering and fruiting, whereas their combination (G-R_1/C-B_1) achieved the earliest development (Fig. 6), highlighting a strong synergistic effect. This synergy extended to yield components (NF/I, NF/C, FSP, and AFW) and overall productivity (EY, TY, and MY), with the GR×SCB interaction explaining approximately 35–45% of the total variance (Table S1). These findings align with previous reports showing that while grafting or bioagents alone may have limited impact, their combination significantly enhances early yield and overall plant performance (Pontes et al. 2024; Curkrov et al. 2021). UG and UC plants consistently exhibited the lowest yield parameters (Figs. 7 and 8), reflecting severe nematode-induced suppression. In contrast, grafts, particularly G-R_1, displayed higher NF/I, NF/C, FSP, AFW (Fig. 7), and overall yield indices (Fig. 8). This enhanced performance is likely attributable to superior root vigor, optimized nutrient uptake, and improved stress tolerance, which collectively facilitate efficient assimilate allocation and reproductive output (Mahmoud 2020; Mahmoud et al. 2025b). These results align with the 'tolerance threshold' concepts established by Duncan and Noling (1998), wherein resistant genetic material shifts the plant's damage function, maintaining productivity despite high nematode pressure. Similarly, SCB treatments (especially C-B_1) improved fruit number and weight (Fig. 7), presumably through plant growth-promoting rhizobacteria that enhance nutrient availability, hormonal balance, and systemic resistance (Adam et al. 2014). Overall, the G-R_1/C-B_1 combination consistently produced the highest yield parameters, confirming that integrating GR with SCB effectively mitigates nematode stress and optimizes tomato productivity. By utilizing these resistant rootstocks in combination with bioagents, we successfully mitigated the yield gaps typically observed under heavy infestation. This integrated approach aligns with the strategies highlighted by Castellano-Hinojosa et al. (2022) as essential pillars for sustainable vegetable production in the post-methyl bromide era.

Fruit quality traits were significantly influenced by all factors, with effects varying by trait and season (Table S1). In 2022, SCB predominantly influenced fruit pH, TSS, and FF, whereas in 2023, GR had a stronger influence on TSS and FF, with FDM and VC consistently governed by GR across seasons (Table S1). Grafts, especially G-R_1, generally outperformed UG controls in quality traits (Fig. 9), indicating enhance physiological resilience, nutrient transport, and metabolic efficiency (Djidonou et al. 2017; Mahmoud 2020; Mahmoud et al. 2025b). Similarly, SCB treatments, particularly C-B_1, improved TSS, FDM, VC, and FF while reducing pH (Fig. 9), indicating modulation of sugar, organic acid, and antioxidant metabolism. Combinations of both rootstocks with C-B_1 coatings (G-R_1/C-B_1 and G-R_2/C-B_1) consistently produced the highest TSS, FDM, VC, and FF, while UG/UC plants had the lowest (Fig. 9), demonstrating the synergistic advantage of integrating GR with SCB.

Leaf pigment contents and root biochemical traits are key indicators of plant physiological status, stress tolerance, and the effectiveness of management practices (Djidonou et al. 2017; Mahmoud et al. 2025a, 2025b). In this study, GR, SCB, and their interaction significantly influenced photosynthetic pigments, with effects varying by pigment type and season (Table S1). The combination of GR, particularly G-R_1, with SCB, especially C-B_1, synergistically enhanced chlorophyll-a, chlorophyll-b, and total carotenoids concentrations (Fig. 10), likely via improved chloroplast function, nitrogen assimilation, and photoprotection (Djidonou et al. 2017; Mahmoud et al. 2025a, 2025b). Conversely, UG/UC controls showed reduced pigment levels under RKN infestation (Fig. 10), associated with increased reactive oxygen species (ROS) accumulation, elevated chlorophyllase activity, and cellular damage (Aissani et al. 2018; Khan et al. 2022; Pratysha 2022).

Similarly, shoot and root biomass, along with root carbohydrates, proteins, and polyphenols, reflected integrated effects on growth, metabolic, and defense, providing a mechanistic basis for assessing plant resilience (Djidonou et al. 2017; Mahmoud et al. 2025a, 2025b). GR primarily enhanced structural growth, with G-R_1 and G-R_2 increasing shoot and root dry matter, whereas UG control consistently showed lower biomass (Fig. 11A–B). SCB, particularly C-B_1, predominantly enhanced root protein, polyphenols, and carbohydrates reserves (Fig. 11C–E), highlighting the responsiveness of root metabolism to organic amendments. The GR×SCB interaction further modified carbohydrate dynamics, indicating that carbon storage is jointly shaped by environmental conditions and treatment quality. High-performing combinations, such as G-R_1/C-B_1 and G-R_2/C-B_1, maximized both biomass and metabolic reserves, whereas UG/UC exhibited the lowest performance (Fig. 11). These results demonstrate that integrating GR with SCB synergistically improves plant growth, metabolic capacity, while susceptible genotypes show constrained growth and biochemical performance.

Severe RKN infection in susceptible 'Apache F_1' plants (UG/UC) induced extensive root galling and egg masses formation (Fig. 1), impairing water and nutrient uptake and triggering ROS accumulation. This oxidative stress accelerated chlorophyll degradation and reduced photosynthetic efficiency, carbohydrate synthesis, and protein accumulation (Aissani et al. 2018; Khan et al. 2022; Pratysha 2022). These physiological constraints translated into stunted vegetative growth (Figs. 2, 3, 4 and 5), delayed reproductive development (Fig. 6), and diminished yield and fruit

quality (Figs. 7, 8 and 9). In contrast, grafting onto resistant hybrids (*Mi*−1/*mi*−1) combined with bioagent seed coating enhanced plant resistance and metabolic activity through complementary mechanisms. The resistant rootstocks provided robust root structural defenses and elevated polyphenols levels (Mahmoud et al. 2025b; Patel et al. 2017), while SCB induced systemic root resistance by further stimulating polyphenol synthesis (Adam et al., 2014; Mahmoud et al. 2025a). Polyphenols mitigated ROS-induced damage and exerted nematicidal activity (Sharma et al. 2025; Pratysha 2022). Collectively these interventions reducing galling and egg-mass formation (Fig. 2), thereby enhancing water and nutrient uptake, photosynthetic pigment content (Fig. 10), and biomass accumulation (Fig. 11). These improvements promoted vigorous vegetative growth (Figs. 3, 4 and 5), accelerated reproductive development (Fig. 6), and enhanced overall yield and quality (Figs. 7, 8 and 9). Variations among GR×SCB combinations likely reflect specific rootstock–microorganism interactions (Sharma et al. 2025), with the combination of rootstock 'Estamino' (R_1) and either bioagent consistently showing superior performance.

Seasonal differences in the magnitude of effects highlights the strong influence of environmental conditions and rootstock-microbe compatibility on treatment efficacy. Variability in treatment responses between seasons likely reflects shifts in microclimatic. Meteorological data (Fig. S1) showed greater climatic fluctuations in 2023, including higher relative humidity and reduced cloud cover, conditions that can intensify both diurnal heat stress and nocturnal chilling stresses. These abiotic stresses reduce photosynthetic efficiency and attenuate *Mi*−1-mediated resistance to RKN (Bajek and Rudolph 2023; Devran et al. 2010; van der Ploeg and Heuvelink 2005). This thermal instability helps explain the observed seasonal differences in RKN suppression (Fig. 1), fruit set (Fig. 7), and quality (Fig. 9). Overall, the performance of GR and SCB performance was closely tied to the environmental context. Their combined application mitigated RKN damage while simultaneously improving growth, yield, and fruit quality, demonstrating their promise as a resilient management strategy under variable agroecological conditions.

Principal component analysis (PCA), a powerful multivariate statistical technique, was employed to identify superior treatment combinations and to elucidate correlations among the measured traits. In this study, PCA reduced 37 variables to three PCs that together explained 97.06% of the total variance (Fig. S2). Trait loadings showed that all measured variables contributed strongly to the first two components (Table 1), underscoring their importance in capturing overall variability. These two components alone accounted for 92.37% of the multidimensional variation, enabling the construction of a biplot the effectively visualized trait correlations, clustered treatment groups, and illustrated their associations with specific variables.

The multivariate analyses provided a coherent overview of trait interrelationships under RKN stress. The PCA biplot (Fig. 12) showed clear clustering among related variables, with traits oriented in the same direction exhibiting positive correlations and those in opposite directions displaying negative associations. These patterns were further validated by Pearson's correlation analysis (Table 2), which revealed strong negative relationships between RKN infection indicators (gall and egg mass numbers) and a wide range of plant performance traits, including vegetative growth, yield and its components, fruit quality attributes, photosynthetic pigments, and root biochemical contents. Such relationships underscore the extensive physiological disruption imposed by RKN, reflecting impaired photosynthetic function, altered carbon and nitrogen metabolism, and reduced biomass accumulation (Banora and Almaghrabi 2019; Khan et al. 2022). These results align with previous reports documenting the suppressive effects of RKN on pigment biosynthesis (Patel et al. 2017), growth, and yield potential (Schomaker et al., 2006; Gharabadiyan et al. 2013; Padilla-Hurtado et al. 2022), as well as the compensatory increase in root polyphenol production under nematode-induced stress (Patel et al. 2017).

The PCA biplot effectively distinguished the treatment groups based on physiological performance, yield attributes, and nematode tolerance. G-R_1/C-B_1 and G-R_1/C-B_2 were closely associated with enhanced productivity, fruit quality, and nematode resistance. Intermediate responses were observed for some treatments, such as UG/C-B_1 and UG/C-B_2, which exhibited moderate performance influenced by both growth and physiological traits.

Conclusion

Integrating grafting onto resistant rootstocks with seed coating using bacterial bioagents proved to be an effective and eco-friendly strategy for managing *M. incognita* in greenhouse-grown tomato. Seed coating with *Sporosarcina psychrophile* Sd4-11 and *Streptomyces scabiei* Wb1n-4 significantly suppressed nematode infection and enhanced plant biochemical defenses. Concurrently, grafting onto the interspecific hybrids 'Estamino' and 'Fortamino' improved vegetative growth, yield, and fruit quality. The synergistic interaction between grafting and these bioagents maximized nematode suppression and productivity, highlighting their complementary roles in sustaining plant health. Overall, this integration offers a robust and sustainable alternative to chemical nematicides for maintaining tomato performance under *M. incognita* infestation in protected cultivation.

Future research should validate these findings under diverse agroecological conditions and elucidate the molecular and physiological mechanisms underlying this synergy, while evaluating a broader range of bioagents and rootstocks to optimize nematode management. Furthermore, targeted studies using qPCR or GFP-dynamics and persistence of these bacterial isolates in the rhizosphere.

Supplementary Information The online version contains supplementary material available at https://doi.org/10.1007/s10725-026-01447-2.

Author contributions Ahmed M.A. Mahmoud: Writing – review & editing, Writing – original draft, Visualization, Validation, Supervision, Formal analysis, Data curation, Conceptualization. Neama H. Osman: Conceptualization, Data curation, Formal analysis, Investigation, Methodology, Writing – original draft. Ahmed A.S.A. El-Eslamboly: Conceptualization, Supervision. Mohamed Adam: Conceptualization, Investigation, Supervision. Mahmoud A.A. Maraey: Investigation, Methodology, Validation, Visualization, Writing – original draft.

Funding Open access funding provided by The Science, Technology & Innovation Funding Authority (STDF) in cooperation with The Egyptian Knowledge Bank (EKB).

Data availability All the data underlying the results are available as part of the article, and no additional source data are required.

Declarations

Competing interests The authors declare no competing interests.

References

Abd-Elgawad MMM (2014) Plant-parasitic nematode threats to global food security. J Nemat 46:130

Abd-Elgawad MMM (2020) Optimizing biological control agents for controlling nematodes of tomato in Egypt. Egypt J Biol Pest Control 30:58. https://doi.org/10.1186/s41938-020-00252-x

Adam M, Westphal A, Hallmann J, Heuer H (2014) Specific microbial attachment to root-knot nematodes in suppressive soil. Appl Environ Microbiol 80:2679–2686. https://doi.org/10.1128/AEM.03905-13

Aissani N, Balti R, Sebai H (2018) Potent nematicidal activity of phenolic derivatives on *Meloidogyne incognita*. J Helminthol 92:668–673. https://doi.org/10.1017/S0022149X17000918

Amorim DJ, Tsujimoto TF, Baldo FB, Leite LG, Harakava R, Wilcken SRS, Gabia AA, Amorim DJ (2024) *Bacillus, Pseudomonas* and *Serratia* control *Meloidogyne incognita* (Rhabditida: Meloidogynidae) and promote the growth of tomato plants. Rhizosphere 31:100935. https://doi.org/10.1016/j.rhisph.2024.100935

Arshad A, Cîmpeanu SM, Jerca IO, Sovorn C, Ali B, Badulescu LA, Drăghici EM (2024) Assessing the growth, yield, and biochemical composition of greenhouse cherry tomatoes with special emphasis on the progressive growth report. BMC Plant Biol 24:1002. https://doi.org/10.1186/s12870-024-05701-s

Aydinli G, Mennan S (2019) Resistance response of tomato cultivars and rootstocks carrying the Mi-1.2 gene to isolates of *Meloidogyne arenaria, M. incognita*, and *M. javanica* at two different growing periods. Hort Sci Technol 37:509–519. https://doi.org/10.7235/HORT.20190051

Ayoub SM (1980) Plant nematology - An agriculture training aid. Nema/Aid Publications, Sacramento, CA, USA, p 195

Bajek V, Rudolph RE (2023) Managing southern root-knot nematode in Kentucky high tunnels using grafted tomato. HortScience 58:704–713. https://doi.org/10.21273/HORTSCI17141-23

Banora MY (2023) Impacting of root-knot nematodes on tomato: Current status and potential horizons for its managing. Tomato Cultivation and Consumption – Innovation and Sustainability. IntechOpen Limited, London, UK, pp 1–22. https://doi.org/10.5772/intechopen.112868

Banora MY, Almaghrabi OAA (2019) Differential response of some nematode-resistant and susceptible tomato genotypes to *Meloidogyne javanica* infection. J Plant Prot Res 59:113–123. https://doi.org/10.24425/jppr.2019.126040

Castellano-Hinojosa A, Noling JW, Bui HX, Desaeger JA, Strauss SL (2022) Effect of fumigants and non-fumigants on nematode and weed control, crop yield, and soil microbial diversity and predicted functionality in a strawberry production system. Sci Total Environ 852:158285.https://doi.org/10.1016/j.scitotenv.2022.158285

Cukrov M, Podrug I, Urlić B, Mandušic M, Žanic K, Radpudić E, Slatnar A, Dumičić G (2021) Effectiveness of grafting and biostimulants application as a strategy for enhancing tomato nematode resistance. Act Hort 1320:283–290.https://doi.org/10.17660/ActaHortic.2021.1320.37

Devran Z, Sögüt MA, Mutlu N (2010) Response of tomato rootstocks with the *Mi* resistance gene to *Meloidogyne incognita* race 2 at different soil temperature. Phytopath Medit 49:11–17.Duncan LW, Noling JW (1998) Agricultural sustainability and nematode integrated pest management. In: Barker KR, Pederson GA, Windham GL, Bartels JM (eds), Plant and Nematode Interactions, Madison: American Society of Agronomy, p. 251–287.https://doi.org/10.2134/agronmonogr36.c13

Djidonou D, Zhao X, Brecht JK, Cordasco KM (2017) Influence of interspecific hybrid rootstocks on tomato growth, nutrient accumulation, yield, and fruit composition under greenhouse conditions. HortTechnology 27:868–877. https://doi.org/10.21273/HORTTECH03810-17

Eissa MM, Abou-Hadid AF, Eissa AM (1996) Relationship between dif's inside and outside plastichouse. Act Hort 434: 279–282.

El-Sappah A, Islam MM, El-Awady HH, Yan S, Qi S, Liu J, Cheng GT, Liang Y (2019) Tomato natural resistance genes in controlling the root-knot nematode. Genes 10:925. https://doi.org/10.3390/genes10110925

Gharabadiyan F, Jamali S, Komeili HR (2013) Determination of rook-knot nematode (*Meloidogyne javanica*) damage function for tomato cultivars. J Agr Sci Belgrade 58:147–157. https://doi.org/10.2298/JAS1302147G

Greco N, di Vito M (2009) Population dynamics and damage levels. Root-Knot Nematodes. CABI, Wallingford, UK, pp 246–274. https://doi.org/10.1079/9781845934927.0246

Grieneisen ML, Aegerter BJ, Stoddard CS, Zhang M (2018) Yield and fruit quality of grafted tomatoes, and their potential for soil fumigant use reduction. A meta-analysis. Agron Sustain Dev 38:29. https://doi.org/10.1007/s13593-018-0507-5

Hooper DJ, Hallman J, Subbotin S (2005) Methods for extraction, processing and detection of plant and soil nematodes. In: Luc, M., Sikora, R.A., Bridge, J. (Eds), Plant Parasitic Nematodes in Subtropical and Tropical Agriculture. Wallingford, CAB International, London, UK, pp. 53–86.

Hunt R (1990) Basic Growth Analysis. Springer, Dordrecht, Germany, 112p. https://doi.org/10.1007/978-94-010-9117-6.

Jiménez-Aguirre MA, Padilla-Hurtado BE, Ceballos-Aguirre N, Cardona-Agudelo LD, Montoya-Estada CN (2023) Antagonist effect of native bacteria of the genus *Bacillus* on the root-knot nematode (Meliodogyne spp.) in tomato germplasm. Chil J Agr Res 83:565–576. https://doi.org/10.4067/s0718-58392023000500565

Johnson RA, Wichern DW (2007) Applied multivariate statistical analysis, 794. 6nd ed. Englewood Cliffs, NJ: Prentice Hall.

Khan MR, Sharma DN, Ahmad I (2022) Temporal impact of root-knot nematode infection on some important biochemical and physiological characters of tomato. Indian Phytopathol 75:749–758. https://doi.org/10.1007/s42360-022-00500-0

Köberl M, Ramadan EM, Adam M, Cardinale M, Hallmann J, Heuer H, Smalla K, Berg G (2013) *Bacillus* and *Streptomyces* were selected as broad-spectrum antagonists against soilborne pathogens from arid areas in Egypt. FEMS Microbiol Lett 342:168–178. https://doi.org/10.1111/1564-6968.12089

Kokalis-Burelle N, Rosskopf EN (2011) Microplot evaluation of rootstocks for control of *Meloidogyne incognita* on grafted tomato, muskmelon, and watermelon. J Nematol 43:166–171

Kyriacou MC, Rouphael Y, Colla G, Zrenner R, Schwarz D (2017) Vegetable grafting: the implications of a growing agronomic imperative for vegetable fruit quality and nutritive value. Front Plant Sci 8:741. https://doi.org/10.3389/fpls.2017.00741

Latimer GW (2012) Official Methods of Analysis of AOAC International, 19th ed. The Association of Official Analysis Chemists International, Maryland, USA, p 1399

Leyva R, Constán-Aguilar C, Blasco B, Sánchez-Rodríguez E, Romero L, Soriano T, Ruíz JM (2013) Effects of climatic control on tomato yield and nutritional quality in Mediterranean screenhouse. J Sci Food Agric 94:63–70. https://doi.org/10.1002/jsfa.6191

Lopes-Caitar VS, Pinheiro JB, Marcelino-Guimarães FC (2019) Nematodes in horticulture: an overview. J Hortic Sci Crop Res 1:106

Mahmoud AMA (2020) Tomato rootstock breeding: evaluation of tomato interspecific hybrid rootstocks under greenhouse conditions. Hortic J 89:575–585. https://doi.org/10.2503/hortj.UTD-199

Mahmoud AMA, El-Eslamboly AASA, Adam M, Maraey MAA (2025a) Biocontrol of *Meloidogyne incognita* and vegetative growth stimulation in tomato 'Moneymaker' plants by Egyptian soil bacteria. Egypt J Biol Pest Control 35:24. https://doi.org/10.1186/s41938-025-00860-5

Mahmoud AMA, Osman NH, El-Eslamboly AASA, Adam M, El-Tawshy MKF, Maraey MAA (2025b) Tomato grafting onto *Solanum nigrum*, *Physalis pubescens*, and interspecific hybrids with *S. habrochaites* for safe production under *Meloidogyne incognita* infestation. S Afr J Bot 184:429–447. https://doi.org/10.1016/j.sajb.2025b.06.011

Melakeberhan H (2004) Physiology, interactions between nematode and their host plants. In: Chen ZX, Chen SY, Dicken DW (eds) Nematode Management and Utilization, Advances and Perspectives, vol Vol 2. CABI International, Wallingford, pp 771–786

Moran R (1982) Formulae for determination of chlorophyllous pigments extracted with *N*,*N*-dimethylformamide. Plant Physiol 69:1376–1381. https://doi.org/10.1104/pp.69.6.1376

Mukherjee A, Mondal P, Sinha Babu SP (2020) Nematode extract-induced resistance in tomato against *Meloidogyne incognita*. Ind J Sci Techn 13:1476–1479. https://doi.org/10.17485/IJST/v13i14.234

Owusu SB, Kwoseh CK, Starr JL, Davies FT (2016) Grafting for management of root-knot nematodes, *Meloidogyne incognita*, in tomato (*Solanum lycopersicum* L.). Nematropica 46:14–21

Padilla-Hurtado B, Morillo-Coronado Y, Tarapues S, Burbano S, Soto-Suárez M, Urrea R, Ceballos-Aguirre N (2022) Evaluation of root-knot nematodes (*Meliodogyne* spp.) population density for disease resistance screening of tomato germplasm carrying the gene Mi-1. Chil J Agr Res 82:157–166. https://doi.org/10.4067/S0718-58392022000100157

Pandey SK, Singh H (2011) A simple, cost-effective method for leaf area estimation. J Bot 2011:1–6. https://doi.org/10.1155/2011/658240

Patel VS, Shukla YM, Dhruye JJ (2017) Influence of root knot nematode (*Meloidogyne* spp.) on phenolic acid profile in root of tomato (*Solanum lycopersicum* L.). Int J Curr Microbiol Appl Sci 6:840–848. https://doi.org/10.20546/ijcmas.2017.610.100

Pontes KB, Machado ACZ, Nogueira AF, Fagundes DFV, de Lima Filho RB, Mosela M, Mian S, Santiago DC, Gonçalves LSA (2024) Efficacy of microbiological nematicides in controlling root-knot nematodes in tomato. Front Agron 6:1462323. https://doi.org/10.3389/fagro.2024.1462323

Potters G, Pasternak TP, Guisez Y, Palme KJ, Jansen MAK (2007) Stress-induced morphogenic responses: growing out of trouble? Trends Plant Sci 12:98–105. https://doi.org/10.1016/j.tplants.2007.01.004

Pratysha S (2022) Phenolic compounds in the plant development and defense: An overview. In: Hasanuzzaman M, Nahar K (eds) Plant Stress Physiology – Perspectives in Agriculture. IntechOpen Lim, London, UK, pp 1–17

Remzeena A, Anitha P (2023) Vegetable grafting: a green technique to combat biotic and abiotic stresses. Vegetos. https://doi.org/10.1007/s42535-023-00752-9

Schomaker CH, Been TH, Viaene N (2006) Distribution patterns of *Meloidogyne* species for the development of sampling strategies. European Society of Nematologists, XXVIII International Symposium 5–9 June 2006, Blagoevgrad, Bulgaria, Programme and Abstracs, 69.

Sharma M, Devi S, Chand S (2025) Biocontrol strategies for sustainable management of root-knot nematodes. Physiol Mol Plant Pathol 136:102548. https://doi.org/10.1016/j.pmpp.2024.102548

Sharma M, Jasrotia S, Ohri P, Manhas RK (2019) Nematicidal potential of *Streptomyces antibioticus* strain M7 against *Meloidogyne incognita*. AMB Express 9:168. https://doi.org/10.1186/s13568-019-0894-2

Singh S, Singh B, Singh AP (2015) Nematodes: a threat to sustainability of agriculture. Proc Environ Sci 29:215–216. https://doi.org/10.1016/j.pronev.2015.07.270

Suzuki M, Umeda H, Matsuo S, Kawasaki Y, Ahn D, Hamamoto H, Iwasaki Y (2015) Effects of relative humidity and nutrient supply on growth and nutrient uptake in greenhouse tomato production. Sci Hortic 187:44–49. https://doi.org/10.1016/j.scienta.2015.02.035

Taylor AL, Sasser JN (1978) Biology, identification and control of root-knot nematodes (*Meloidogyne* Species). A Cooperative Publication of North Carolina State University, Dept. of Plant Pathology, and USAID, Raleigh, NC, USA. 111pp.

Taylor AL (1967) Introduction to research on plant nematology. An FAO guide to the study and control of plant-parasitic nematodes. Food and Agricultural Organization of the United Nations, Rome. 133p.

Taylor DP, Netscher C (1974) An improved technique for preparing perineal patterns of *Meloidogyne* spp. Nematologica 20:268–269

van der Ploeg AVD, Heuvelink E (2005) Influence of sub-optimal temperature on tomato growth and yield: a review. J Hortic Sci Biotechnol 80:652–659. https://doi.org/10.1080/14620316.2005.11511994

Viljoen JJF, Labuschagne N, Fourie H, Sikora RA (2019) Biological control of the root-knot nematode *Meloidogyne incognita* on tomatoes and carrots by plant growth-promoting rhizobacteria. Trop Plant Pathol 44:284–291. https://doi.org/10.1007/s40858-019-00283-2

Wickens TD, Keppek G (2004) Design and Analysis: A Researcher's Handbook. Pearson Prentice-Hall, New Jersey, USA, p 624

Yan W, Kang MS (2003) GCE-Biplot Analysis: A Graphical Tool for Breeders, Geneticists, and Agronomists. CRC Press, New York, USA

Zandalinas SI, Mittler R, Balfagón D, Arbona V, Gómez-Cadenas A (2018) Plant adaptations to the combination of drought and high temperatures. Physiol Plant 162:2–12. https://doi.org/10.1111/ppl.12540